HYDRODYNAMICS OF TWO-PHASE FLOW IN A TRICKLE BED REACTOR

A Thesis

by

PUNEET KAWATRA

Submitted to the Office of Graduate and Professional Studies of
Texas A&M University
in partial fulfillment of the requirements for the degree of

MASTER OF SCIENCE

Chair of Committee,   Benjamin A. Wilhite
Committee Members,   Mahmoud M. El-Halwagi
                      Karen Vierow Kirkland
Head of Department,   M. Nazmul Karim

August 2017

Major Subject: Chemical Engineering

ABSTRACT

Hydrodynamic data from large trickle bed columns are scarce. In this study, pressure drop, liquid holdup, and transition from low interaction regime to high interaction regime were investigated in a pilot-scale trickle bed column of 13 in. inner diameter and 8 ft. bed height, using air-water system at atmospheric pressure. Data were collected in the low gas superficial velocity range, which has not been covered extensively in literature. Gas flow rate was varied from 0 to 400 SLPM (standard liter per minute), i.e., 0 – 70 mm/s, and liquid flow rate was varied from 0 to 60 gpm (gallons per minute), i.e., 0 – 45 mm/s. The system was prewetted in high interaction regime before taking each measurement. Pressure and liquid load were measured using sensors, while flow regime transition was observed visually and by noting the standard deviation in pressure drop.

The aim of this study is to record and analyze hydrodynamic data that can closely match that of industrial-scale reactors. The experiments showed hysteresis, indicating multiplicity of hydrodynamic states. For experiments following a consistent prewetting procedure, significant deviation was observed from the pressure drop and liquid holdup correlations in literature. At lower liquid flow rates, flow is gravity driven, while drag forces come into play as liquid flow is increased. In addition, at higher liquid flow rates, liquid holdup is overestimated by correlations from studies on lab-scale trickle bed columns. Lastly, flow regime transition agreed with existing flow maps in literature, with the observation of local pulsing in the bed.

DEDICATION

To

My Family

ACKNOWLEDGEMENTS

CONTRIBUTORS AND FUNDING SOURCES

NOMENCLATURE

Notation

L'	Mass Flux of liquid, $kg/(m^2\text{-}s)$
G'	Mass Flux of gas, $kg/(m^2\text{-}s)$
L	Liquid Flow Rate, gpm
G	Gas Flow Rate, SLPM
$\frac{\Delta P}{L}$	Frictional pressure drop per unit length of bed, psi/ft
v	Superficial velocity, mm/s
D_p	Particle diameter, m
D_C	Column Diameter, m
Re	Reynolds Number, dimensionless
We	Weber Number, dimensionless
Ga	Galileo Number, dimensionless
f_{lg}	Two-phase friction factor, dimensionless
a_v	Bed surface area per unit bed volume, m^2/m^3
Eö	Eötvös number, dimensionless

Greek Letters

$\beta_T, \beta_S, \beta_D$	Total, Static and Dynamic Liquid Saturation, %
ε	External porosity of catalyst bed
μ	Viscosity, kg/m-s

ρ	Density, lb_m/ft^3
σ	Surface Tension, lb_f/in
δ	Pressure drop with gravity term, psi/ft
χ, φ	Two-phase flow parameters, dimensionless
σ_R	Relative Standard Deviation

TABLE OF CONTENTS

LIST OF FIGURES

x

CHAPTER I

INTRODUCTION AND LITERATURE REVIEW

I.1. General

Trickle bed reactors are three-phase flow reactors, in which gas and liquid phases flow through a packed bed of solid catalyst. Employing a trickle bed reactor minimizes the energy costs associated with vaporization of the reactants [1]. Most Trickle bed reactors in the industry are co-current down-flow reactors with both gas and liquid flowing downwards in the direction of gravity. Co-current downflow reactors have various advantages over co-current upflow or counter-current flow, such as lower pressure drop, lesser catalyst attrition, and lower chances of flooding. This allows for operations across a wider range of operating conditions, with a lower pumping load requirement and a nearly uniform partial pressure of reactants across the length of the catalyst bed [1-3].

Trickle-bed reactors are used extensively in the refining, petrochemical, waste-treatment and pharmaceutical industries to produce fuels and chemicals. A few examples of diverse three-phase reactions carried out in Trickle Bed Reactors are mentioned below:

i. Hydrogenation of many types of chemical compounds such as Naphthalene [4], 1,5-cyclooctadiene [5], diols[6], alpha-methylstyrene [7], phenylacetylene [8], olefins [9], acetophenone [10], unsaturated fats [1]

1

ii. Oxidation of Ethyl Alcohol [11], Sulfur Dioxide [12], BTX (Benzene, Toluene, and Xylene) [13], acetic acid [14], formic acid [15]

iii. Hydration of 2-methyl-2-butene [16], iso-butene [17]

iv. Residuum Hydrotreating, Desulfurization and Denitrification [9]

v.   Hydrocracking of heavy gas oils to middle distillates [9]

vi. Isomerization of cyclopropane to propylene [18]

vii. Synthesis of compounds like calcium acid sulpfite (Jenssen tower operation), butynediol, sorbitol, etc. [1]

The two major transport phenomena in such systems involve (1) mass transfer between the fluids and solid phase (catalyst), which plays an important role in reaction kinetics, and (2) solid-fluid heat transfer, which plays an important role in effectively supplying heat to the catalyst for endothermic reactions, or removing heat for exothermic reactions to avoid overheating of the catalyst. The ultimate goal of a trickle bed reactor is to achieve the desired conversion of reactants, which may involve operating in conditions that facilitate higher heat and mass transfer, while at the same time maintaining a stable and economically viable operation. This requires a careful study of the hydrodynamics of multi-phase flow due to the complexities associated with liquid-solid-gas interaction in a packed bed.

I.2. Hydrodynamics

Understanding the hydrodynamics of Trickle Bed Reactors is key to their effective design and performance prediction [19]. Dudukovic and Mills [20] summarized the macroscale and microscale phenomena of interest occurring in Trickle Bed Reactors.

They suggested that the hydrodynamics in such reactors should be described through a mechanistic approach rather than a complex fundamental viewpoint. The performance of a Trickle Bed Reactor can therefore be characterized based on a certain set of macroscopic hydrodynamic parameters, including, but not limited to, the following:

      i.   Flow regime

      ii.   Pressure drop

      iii.   Liquid holdup

      iv.   Liquid-solid contacting

The role of all these factors should be quantitatively evaluated for a successful scale-up of pilot plant data [21]. This research focusses on the first three parameters, all of which can be directly observed and analyzed through experiments.

Table 1 summarizes some popular experimental studies done on trickle bed reactors and examined as a part of this thesis. This is followed by a description of various hydrodynamic parameters studied in this research, and a closer look at some selected publications that have proposed flow maps and correlations for pressure drop and liquid saturation based on experimental data.

Table 1: Literature Review

Reference	Information	Gas-Liquid System	Packing	Column Dimensions
Larkins et al, 1961 [22]	Pressure Drop & Liquid Holdup Correlation	Air-water, and other fluids	Spheres (3/8", 3mm), Cylinders (1/8")	2" and 4" ID, 7 ft. height
Turpin et al, 1967 [23]	Pressure Drop & Liquid Holdup (All flow regimes)	Air-water	0.3" tabular alumina	2", 4" and 6" diameter, 7ft high columns
Satterfield et al, 1972 [18]	Liquid Holdup (Low interaction regime)	Air-water	Glass Spheres (3mm), Porous Cylinders (3.2 mm x 3.2 mm, 1.6 mm x 8 mm)	28 mm ID, 33 cm height
Sato et al, 1973 [24] [25]	Pressure Drop & Liquid Holdup Correlation, Flow map	Air-water	Glass spheres (2.59-16.5 mm)	122mm and 65.8 mm ID
Charpentier & Favier, 1975 [26]	Flow Regime Transition Map, Pressure Drop & Liquid Holdup Correlation	Air-water, hydrocarbons	Sphere(3 mm), Cylinder (1.8x6mm, 1.4x5mm)	5/10 cm ID 1.2 m length
Midoux, Favier and Charpentier, 1976 [27]	Pressure Drop & Liquid Holdup Correlations for foaming and non-foaming liquids	Air-water, hydrocarbons	Sphere(3 mm), Cylinder (1.8x6mm, 1.4x5mm)	5/10 cm ID 1.2 m length
Colombo et al, 1976 [21]	Liquid Holdup (Low interaction regime)	Air-water	Porous Cylinders (0.38x0.48 cm)	3 cm ID, 1 m packing height
Specchia et al, 1977 [28]	Liquid Holdup (High and Low Interaction Regimes)	Air-water, and other liquids	Glass Spheres (6mm), Cylinders (5.4 mmx5.4 mm, 2.7 mmx2.7 mm)	0.08 m diameter, 1.05 m height
Chou et al, 1977 [29]	Trickle-to-pulse flow transition	Air-water, and other liquids	2.9 cm glass beads	63.5 mm ID 1.78 m length

Table 1 Continued.

Reference	Information	Gas-Liquid System	Packing	Column Dimensions
Fukushima et al, 1977 [30]	Flow Map, Liquid Holdup	Air-Water	3/8" raschig rings 1/2" and 1" spheres	11.4/20 cm ID 1.4/1.9 m length
Clements et al, 1980 [31] [32]	Pressure Drop & Liquid Holdup Correlation (Trickle & Pulsing Flow)	Air-silicone	1.04 mm, 1.39 mm, 3.35 mm extrudates	55 mm ID and 1.5 m length
Mills et al, 1981 [33]	Liquid holdup and contacting efficiency	Hexane-Helium	0.0718 cm porous alumina	1.35 cm ID, 40 cm length
Blok et al, 1983 [34]	Correlation for flow transition, liquid holdup and Pressure Drop	Air-water and several other liquids	Raschig Rings (2.5 and 4 mm)	5, 10 and 20 cm ID 1m length
Levec et al, 1986 [35]	Pressure Drop & Liquid Holdup Correlation	Air-water	Glass spheres (0.3 and 0.6 cm diameter)	17.2 cm ID, 130 cm length
Ellman et al, 1988 [36]	New Pressure Drop Correlations for Industrial Reactors	Air-water, and other liquids	Spheres and cylinders (1.16-3.06 mm)	23-100 mm ID, 0.49 - 2 m height
Wammes et al, 1990 [37] [38]	Liquid Holdup correlation at low gas velocities, flow regime transition	Water/ethyle neglycol, nitrogen	Glass spheres (3 mm)	51 mm ID, 1 m length
Wang et al, 1994 [39]	Trickle-to-pulse flow transition	Air-water and other liquids	2.7 mm, 4 mm and 8 mm spherical glass beads	70mm ID, 1000 mm height
Honda et al, 2015 [40]	Trickle-to-Pulse and Trickle-to-bubbly flow transition	Air-Water	3.41 mm spherical beads	2" ID and 36" height

I.2.1. Flow Regime

A trickle bed reactor can be operated in a variety of flow regimes (Figure 1), broadly classified as 'Low Interaction Regime' and 'High Interaction Regime'. The mixing characteristics and heat and mass transfer phenomena within the reactor strongly depend on the operating flow regime [1]. Transition from one flow regime to another may differ for foaming and non-foaming systems, along with other hydrodynamic parameters [29, 41].

As the name suggests, foaming systems involve liquids that begin to foam at sufficiently high flow rates, in the presence of a gas flow rate. For example, hydrocarbons like kerosene, desulfurized and non-desulfurized gas oils have a tendency to foam, whereas cyclohexane, gasoline, and petroleum ether do not [26]. In industry practice, some hydrocarbon systems may begin to foam depending on properties such as surface tension and viscosity, and anti-foaming agents or defoamers are usually added to inhibit foam formation [41]. Therefore, many studies in literature use non-foaming systems in experiments. Since air and water have been as fluids in this experimental study, the scope of this study only extends to non-foaming systems only.

Following classification of flow regimes exists in a non-foaming system:

i.   *Low Interaction Regime:*

Also known as the Trickle Flow regime, this flow behavior is observed at low liquid and gas flow velocities. Liquid phase trickles down in the form of rivulets and thin films over the packing, interacting minimally with the continuous gas phase. This flow regime enables stable operation of the reactor and ensures high residence time as

6

required by kinetics-limited reactions. However, in some cases, trickle flow operation may not achieve the desired reactor performance due to low heat and mass transfer coefficients.

ii. *High Interaction Regime:*

This is further classified into three regimes:

a. Pulse Flow: This is characteristic of high liquid and gas flow velocities, and results in significant interaction between the fluids and the solid catalyst. At high liquid flow rates, the catalyst bed is substantially wetted, leading to the formation of bridges of liquid phase between the catalyst particles. These bridges grow in size till the time they are broken and pushed down by the gas flowing through the bed. As a result, alternating liquid and gas rich slugs (or "pulses") are observed flowing through the catalyst bed. This leads to fluctuations in liquid holdup and pressure drop in the column, as well as in heat and mass transfer rates. Operation in pulsing regime, albeit conducive to high heat transport coefficients, is unfavorable owing to the instability in operation associated with the fluctuations in the column.

b. Dispersed Bubble Flow: At low gas velocities and high liquid to gas flow ratios, gas phase is broken down into small dispersed bubbles flowing through a continuous liquid phase. This too results in a high level of interaction and is accompanied by rapid fluctuations in the column hydrodynamic parameters.

c. Spray Flow: Spray or mist flow is achieved at very high gas to liquid flow ratios, wherein liquid is broken down into tiny drops entrained in the downward continuous gas flow. This regime is not very common in the industry because most reactions require higher liquid to gas flow ratios. Since it is hard to discern a boundary between spray flow regime and trickle flow regime, both are sometimes grouped together and termed as 'gas continuous flow' regime [24, 42].

While it is useful to operate in trickle flow regime in order to achieve high liquid residence time and stable operation, operating the reactor in pulsing regime can be more suitable for mass transfer limited reactions, where high heat and mass transfer coefficients are desired [2]. A majority of industrial columns thus operate in the trickle flow regime, or close to the boundary of trickle-to-pulse flow regime [40, 43]. Prediction of flow regime transition is important in reactor design, as many critical parameters like pressure drop, liquid holdup, and mass transfer coefficients are dependent on the flow regime. Therefore, significant research has focused on identifying the transition from trickle flow to pulse flow or bubble flow, and on quantifying the associated hydrodynamic parameters. Many authors have proposed flow maps and correlations to identify transition from one regime to another. For example, Figure 1 shows the first flow map proposed by Charpentier & Favier, 1975 that is accepted widely in literature. It is based on Baker coordinates, in which the dimensionless group $L\lambda\varphi/G$ is plotted against G/λ, where λ and φ are parameters dependent on fluid properties. Each of these parameters equals 1 when the fluids are air and water.

8

(i) **(ii)**
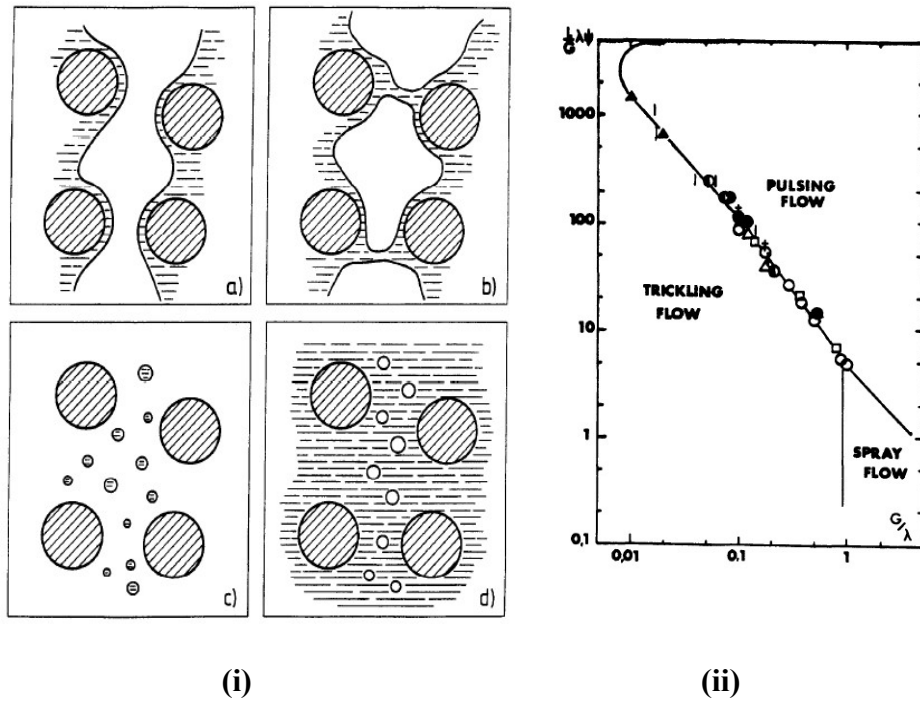
Figure 1. (i) Flow regimes in a trickle bed reactor: a) trickle flow b) pulse flow c) spray flow d) dispersed bubble flow [44] (ii) Flow map proposed by Charpentier & Favier, 1975 [26]

I.2.2. Pressure Drop

Pressure drop calculations are important for Trickle Bed Reactors for the estimation of feed pressure for pumping cost estimation, and for predicting parameters like liquid holdup, wetting efficiency, and transport coefficients [1, 3, 20, 45]. A large number of correlations and theoretical models can be found in literature for prediction of two-phase pressure drop through a packed bed. For this study, focus is on correlations that are based on experimental work. A majority of the correlations are based on some form of the Ergun equation [46] or a similar equation, combined with a number of two-

9

phase parameters. Some correlations are purely empirical in nature, while others are semi-empirical and employ dimensionless parameters of physical significance.

The Ergun equation predicts single-phase pressure drop through a packed bed:

$$\frac{\Delta P}{L} = 150 \frac{(1-\epsilon)^2}{\epsilon^3} \frac{u\mu}{D_p{}^2} + 1.75 \frac{(1-\epsilon)}{\epsilon^3} \frac{u^2\rho}{D_p} \tag{1}$$

Below is a summary of a few commonly used correlations:

i.   *Larkins et al, 1961 [22]*

Energy Balance of a flow system through a packed bed gives the following expression:

$$\frac{\int dP}{\rho} + \frac{\Delta u^2}{2} - (\Delta L)(\frac{g}{g_c}) + \Sigma F + W_S = 0 \tag{2}$$

On neglecting the shaft work, density changes and kinetic energy change through the bed, we arrive at the following expression for a fully developed flow:

$$-\frac{\Delta P}{L} + \rho\left(\frac{g}{g_c}\right) = \frac{(\Sigma F)\rho}{\Delta L} = \delta \tag{3}$$

Two-phase parameters ϕ and χ were proposed by Lockhart and Martinelli [47] in 1949 for flow in open tubes. These were further extended to packed beds by Larkins and White, and since then, have been extensively used as a basis for predicting two-phase pressure drop in packed beds. Below are the aforementioned two-phase parameters:

$$\chi = \sqrt{\left(\frac{\delta_l}{\delta_g}\right)} \tag{4}$$

$$\phi_g = \sqrt{\left(\frac{\delta_{lg}}{\delta_g}\right)} \qquad (5)$$

$$\phi_l = \sqrt{\left(\frac{\delta_{lg}}{\delta_l}\right)} \qquad (6)$$

where, δ_{lg} is the two phase pressure drop, while δ_l and δ_g are liquid and gas-phase

pressure drops, respectively, that would exist if they were flowing separately in a single-

phase flow with the same flow rate as in the two-phase flow.

Larkins and White used a form of Ergun equation for single-phase pressure drop

and then proposed a correlation to calculate the two-phase pressure drop:

$$\delta \left(\frac{g_c \rho D_p{}^3}{\mu^2}\right) \left(\frac{\epsilon}{1-\epsilon}\right)^3 = Re(\alpha + \beta Re) \qquad (7)$$

$$log_{10}\left(\frac{\delta_{lg}}{\delta_l + \delta_g}\right) = \frac{0.416}{((log_{10}X)^2 + 0.666)} \qquad (8)$$

where,

$$Re = \frac{\rho v D_p}{\mu(1-\epsilon)} \qquad (9)$$

$$D_p = 6\frac{(1-\epsilon)}{a_v} \qquad (10)$$

α, β are packing-specific constants, and $0.05 < \chi < 30$

ii.   *Turpin and Huntington, 1967 [23]*

Turpin and Huntington proposed the following empirical pressure drop

correlation that is not dependent on knowledge of single-phase pressure drop.

$$\ln f_{lg} = 7.96 - 1.34 \ln Z + 0.0021(\ln Z)^2 + 0.0078\,(\ln Z)^3 \qquad (11)$$

$$f_{lg} = \delta_{lg} D_e / 2 u_G^2 \rho_G \tag{12}$$

$$D_e = \frac{2}{3} D_P \frac{\epsilon}{1 - \epsilon} \tag{13}$$

$$0.2 < Z = \frac{Re_G^{1.167}}{Re_L^{0.767}} < 500$$

The frictional pressure drop is correlated to the two-phase friction factor f_{lg}, which is expressed as a function of a dimensionless two-phase parameter Z.

iii.   *Sato et al, 1973 [24]*

Instead of the Ergun Equation, Sato et al used a non-linear formula of Tallmadge [48]:

$$f_v = 150 + 4.2 Re^{5/6} \tag{14}$$

where, f_v is the viscous flow factor, given by:

$$f_v = \left(\frac{\Delta P}{L}\right) \frac{g_c D_p^2}{\mu U} \frac{\epsilon^3}{(1 - \epsilon)^2} \tag{15}$$

The pressure drop was thus represented by the following correlation:

$$\phi_l = 1.30 + \frac{1.85}{\chi^{0.85}} \tag{16}$$

where, $0.1 \leq \chi \leq 20$

An alternate expression for pressure drop was proposed, resembling the one by Larkins et al:

$$log_{10}\left(\frac{\Delta P_{lg}}{\Delta P_l + \Delta P_g}\right) = \frac{0.70}{[(log_{10}(\chi/1.2)]^2 + 1.0)} \tag{17}$$

iv.   *Midoux, Favier and Charpentier, 1976 [27]*

Midoux et al performed a similar analysis as Larkins and White, using a modified form of Ergun equation for single-phase pressure drop. The equation employed packing specific parameters A' and B'.

$$\frac{\Delta P}{L} = A'\mu\left(\frac{G'}{\rho}\right) + B'\left(\frac{G'^2}{\rho}\right) \tag{18}$$

Here, G' is the gas mass flux in kg/m^2-s. A similar equation for liquid phase was used. Parameters A' and B' specific to our packing were calculated based on the Ergun equation.

The pressure drop was represented by the following correlation:

$$\phi_l = 1 + \frac{1}{\chi} + \frac{1.14}{\chi^{0.54}} \tag{19}$$

where, $0 \leq \chi \leq 80$

v.   *Specchia and Baldi, 1977 [28]*

This study presented new form of correlations, based on different hydrodynamic regimes. Specchia and Baldi proposed that the correlations of pressure drop and liquid holdup should be different for different flow regimes, because of different levels of gas-liquid interaction. For low interaction regime, pressure drop is calculated as that due to gas flowing in a bed restricted by the presence of liquid, thereby considering the influence of liquid holdup in the co-current gas flow. Shown below is the correlation

13

proposed for low interaction regime, which involves an Ergun-type equation, taking into account static and dynamic liquid holdup (β_S and β_D, respectively):

$$\delta_{lg} = k_1 \frac{[1 - \epsilon(1 - \beta_S - \beta_D)]^2}{\epsilon^3(1 - \beta_S - \beta_D)^3} \mu_G u_G + k_2 \frac{1 - \epsilon(1 - \beta_S - \beta_D)}{\epsilon^3(1 - \beta_S - \beta_D)^3} \rho_G u_G \qquad (20)$$

where, k_1 and k_2 are packing dependent coefficients evaluated experimentally.

For pressure drop estimation in high interaction regime (pulsing flow), a separate correlation was proposed on an empirical basis, very similar to that proposed by Turpin and Huntington, 1967 [23]:

$$\ln f_{lg} = 7.82 - 1.30 \ln\left(\frac{Z}{\psi^{1.1}}\right) - 0.0573 \left[\ln\left(\frac{Z}{\psi^{1.1}}\right)\right]^2 \qquad (21)$$

$$0.6 < \frac{Z}{\psi^{1.1}} < 500$$

$$\Psi = \frac{\sigma_W}{\sigma_L} \left[\frac{\mu_L}{\mu_W}\left(\frac{\rho_W}{\rho_L}\right)^2\right]^{\frac{1}{3}} \qquad (22)$$

vi.   Ellman et al, 1988 [36]

The authors proposed a new correlation for two-phase pressure drop, based on experiments performed over a wide range of fluid properties and packing geometries. The correlations developed were proposed to be applicable to industrial trickle bed reactors. The friction factor, as specified in the correlation by Turpin & Huntington, is given by

$$f_{lg} = \delta_{lg} D_P / 2 u_G^2 \rho_G \qquad (23)$$

The friction factor can be found by the following correlation:

$$f_{lg} = A(\chi_G \xi_1)^j + B(\chi_G \xi_1)^k \quad \text{(High Interaction Regime)} \qquad (24)$$

14

$$f_{lg} = C(\chi_G\xi_2)^m + D(\chi_G\xi_2)^n \quad \text{(Low Interaction Regime) (25)}$$

where,

$$\xi_1 = \frac{Re_L^{0.25}We_L^{0.2}}{(1 + 3.17Re_L^{1.65}We_L^{1.2})^{0.1}} \tag{26}$$

$$\xi_2 = \frac{Re_L^2}{(0.001 + Re_L^{1.5})} \tag{27}$$

A = 6.96; B = 53.27; C = 200; D = 85; j = -2; k = -1.5; m = -1.2; n = -0.5

χ_G is a factor derived from the two-phase flow factor χ, and is given by:

$$\chi_G = \left(\frac{We_G}{We_L}\right)^{0.5} \tag{28}$$

The Weber number incorporates the interfacial forces between the liquid and the gas phase, while the Reynolds number incorporates the viscous force inside the liquid. Therefore, the correlation for Low Interaction regime ($\chi_G < 0.8$) includes only the Reynolds number, while for High Interaction Regime ($1.2 < \chi_G$) it includes both the Reynolds and Weber numbers.

I.2.3. Liquid Holdup/Saturation

Liquid holdup, defined as the amount of liquid present in the column at any given point of time, is expressed as a fraction of the column volume. Another commonly used term is liquid saturation, which is the fraction of available void volume in the packing occupied by the liquid. In this thesis, the correlations mentioned will be used for the calculation of liquid saturation, but the two terms may be used interchangeably while theoretically referring to the parameter. Liquid saturation is an important hydrodynamic parameter in a trickle bed reactor, because (1) it controls the residence time of the liquid

in the packing, which can be used to size the reactor, and which eventually controls the overall conversion in the reactor, and (2) it gives an indication of the extent of liquid-solid contacting and the pressure gradient in the bed, which affect the overall heat and mass transfer rates in the bed. Liquid Saturation can be divided into two categories:

    i.   Static Liquid Saturation (β_S), which is the liquid that remains in the bed after complete draining, and

    ii.   Dynamic Liquid Saturation (β_D), which is the liquid that continuously drains out and gets replenished

Both combined together constitute the total liquid holdup. For porous catalysts, total liquid holdup comprises of liquid contained in the void volume external to the packing (external holdup) as well as that inside the pores of the catalyst (internal holdup). For the purpose of this study, in which non-porous packing is employed, the external liquid holdup is equal to the total liquid holdup.

Static liquid holdup, also known as residual or capillary holdup, usually represents only a small fraction of the total holdup, and is independent of the previous operating conditions. Charpentier et al (1968) [49] proposed that the static holdup is a function of the ratio between gravitational and capillary forces, represented by the Eötvös number:

$$E\ddot{o} = \rho_l g D_P^2 / \sigma_l \tag{29}$$

At Eö < 5, value of $\varepsilon\beta_S$ is about 0.05, while at higher values of Eö, static liquid saturation is inversely proportional to the Eötvös number. While static liquid holdup is a function of liquid properties and packing shape size and wettability, dynamic holdup is a

16

function of liquid and gas properties, reactor pressure, flow rates, and packing characteristics [50].

Similar to pressure drop estimation, many studies have been done to predict liquid saturation in a trickle bed reactor. Since the forces behind static and dynamic holdup are different, many of these correlations consider them separately, and only predict the dynamic liquid saturation, while some others predict the total liquid saturation. The complexities associated with flow patterns, packing structure, and particle wettability, are some of the challenges associated with accurately predicting liquid saturation for a wide range of flow rates and a variety of packing types [37]. For low interaction regimes, liquid holdup has usually been proposed to be a function of Reynolds Number Re_L, the Galileo Number Ga_L, and a packing dependent parameter. For high interaction regime, more dimensionless parameters come into play to account for higher pressure drop, higher energy dissipation, additional gas-liquid interaction, and/or surface tension forces [20]. Following list presents some selected publications that propose predictive correlations based on experimental data:

    i.   *Otake and Okada, 1953 [51]*

This is one of the initial works that introduced the role of the Reynolds Number (Re) and Galileo Number (Ga) in liquid holdup correlations. This correlation was introduced for single phase free trickling liquid and is extended to two-phase flow with low gas velocities:

For Spheres, $10 < Re < 2000$

$$\epsilon\beta_D = 1.295(Re)^{0.676}(Ga)^{-0.44}(a_v D_P) \tag{30}$$

17

For Raschig Rings and Broken Solids,

$$\epsilon\beta_D = 15.1(Re)^{0.676}(Ga)^{-0.44}(a_vD_P)^{-0.6} \qquad (31)$$

$$10 < Re < 2000$$

$$\epsilon\beta_D = 21.1(Re)^{0.51}(Ga)^{-0.44}(a_vD_P)^{-0.6} \qquad (32)$$

$$0.01 < Re < 10$$

where,

$$Re = \frac{\rho v D_p}{\mu(1-\epsilon)}$$

$$Ga = \frac{D_P^3 \rho_L^2 g}{\mu_L^2} \qquad (33)$$

However, these correlations were based on absorption columns packed with large particles, and may not fit the data as particle size is reduced [52].

ii. *Larkins et al, 1961 [22]*

The dynamic liquid saturation is correlated by the following expression:

$$log\beta_D = 0.525log\chi - 0.109(log\chi)^2 - 0.774 \qquad (34)$$

$$0.05 < \chi < 30$$

where the parameters are as defined in Section I.2.2. (i).

iii. *Turpin and Huntington, 1967 [23]*

Turpin and Huntington proposed the following empirical correlation for dynamic liquid saturation that does not contain any term for packing characteristics.

$$\beta_D = -0.017 + 0.132\left(\frac{L'}{G'}\right)^{0.24} \qquad (35)$$

$$1.0 < \left(\frac{L'}{G'}\right)^{0.24} < 6.0$$

iv.   *Satterfield et al, 1972 [18]*

Satterfield and Way proposed a correlation for total liquid saturation at low gas flows, for free trickling liquid:

$$\epsilon\beta_T = Au_L^{1/3}\mu_L^{1/4} + B \tag{36}$$

where, A and B are dependent on the packing type. As can be seen from the correlation, liquid holdup at low gas flows is proposed to be independent of the gas flow. This form of a correlation is usually applied to small range of gas flows in lab scale experiments – it fails for commercial operations because of higher gas flows and thus, lower holdup values [26].

v.   *Sato et al, 1973 [24]*

Sato et al correlated the total liquid saturation with the two-phase parameter χ as defined in Section I.2.2. (i):

$$\beta_T = 0.4\chi^{0.22}a_v^{1/3} \tag{37}$$

where, $0.1 \leq \chi \leq 20$

Here, a_v is the specific surface area of the bed and is given by

$$a_v = \frac{6(1-\epsilon)}{D_P} \tag{38}$$

19

vi.   Charpentier and Favier, 1975 [26]

Charpentier and Favier correlated the total liquid saturation as a function of a

modified two-phase parameter χ':

$$log\beta_T = -0.363 + 0.168 log\chi' - 0.043(log\chi')^2 \tag{39}$$

$$\chi' = \left[\frac{\frac{L'}{G'}}{\left(\frac{1}{\rho g_c} \cdot \frac{\Delta P}{L} + 1\right)}\right]^{0.5} \tag{40}$$

$$0.05 < \chi' < 100$$

Here, χ' is the ratio of the frictional energy flux dissipated when liquid is

trickling through the packing, to that when gas is flowing through the packing.

The corresponding pressure drop as used in the correlation is calculated by the

following expression:

$$\frac{\Delta P}{L} = \frac{h_k a_g^2 (1-\epsilon)^2}{\epsilon^3} u\mu + \frac{h_B a_g (1-\epsilon)}{\epsilon^3} \rho u^2 \tag{41}$$

where, h_k and h_B are packing dependent coefficients.

vii.   Goto and Smith, 1975 [52]

The results and the corresponding liquid saturation correlation by Goto and

Smith matched those of Satterfield et al. In this case, however, the dynamic saturation

was correlated instead of total saturation:

$$\epsilon\beta_D = A u_L^{1/3} \mu_L^{1/4} \tag{42}$$

where, A is a packing dependent coefficient.

viii.   Midoux, Favier and Charpentier, 1976 [27]

Midoux et al correlated the total liquid saturation with the two-phase parameter χ as defined in Section I.2.2. (i):

$$\beta_T = \frac{0.66(\chi)^{0.81}}{1 + 0.66(\chi)^{0.81}} \tag{43}$$

where, $0 \leq \chi \leq 80$

ix.   *Specchia and Baldi, 1977 [28]*

For low interaction regime, Specchia and Baldi assumed that the mechanism of momentum transfer between the trickling flow and the packing was not significantly affected by the co-current gas flow. The dynamic saturation β_D for free trickling flow with zero gas flow, was correlated as below, similar to the expression introduced by Otake and Okada [51]:

$$\beta_D = 3.86(Re_L)^{0.545}(Ga)^{-0.42}\left(\frac{a_v D_P}{\epsilon}\right)^{0.65} \tag{44}$$

$$0.3 < Re_L < 300$$

When there is a co-current gas flow, the pressure gradient and the accompanying gas-liquid drag forces induce an additional acceleration on the liquid. Therefore, a modified Galileo number Ga* was defined, such that:

$$Ga^* = \frac{D_P^3 \rho_L (\rho_L g + \delta_{\text{LG}})}{\mu_L^2} \tag{45}$$

This gave rise to a general correlation for two-phase flow in poor interaction regime:

$$\beta_D = 3.86(Re_L)^{0.545}(Ga^*)^{-0.42}\left(\frac{a_v D_P}{\epsilon}\right)^{0.65} \tag{46}$$

$$3 < Re_L < 470$$

For liquid saturation in high interaction regime (pulsing flow), a separate correlation was proposed using the same parameter 'Z' as used in their pressure drop correlation:

$$\beta_D = 0.0125 \left[\frac{Z}{\Psi^{1.1}}\right]^{-0.312} \left(\frac{a_v D_P}{\epsilon}\right)^{0.65} \tag{47}$$

$$1 < \frac{Z}{\Psi^{1.1}} < 500$$

x.   *Dudukovic and Mills, 1981 [33]*

Dudukovic and Mills introduced the following correlations that asymptotically reach a value of 1 at high liquid velocities:

$$\beta_D = 1.0 - exp(-0.634 Re_L^{-0.333} Fr_L^{0.842} We_L^{-0.448} \left(a_v \left(\frac{D_P}{\epsilon}\right)^2\right)^{1.086}) \tag{48}$$

$$\beta_D = tanh(0.731 Re_L^{-0.333} Fr_L^{0.708} We_L^{-0.346} \left(a_v \left(\frac{D_P}{\epsilon}\right)^2\right)^{0.924}) \tag{49}$$

$$0.3 < Re_L < 32$$

$$Fr_L (Froude\ number\ for\ liquid) = a_v L^2 / \rho_L^2 g \tag{50}$$

$$3.0\ X\ 10^{-5} < Fr_L < 2.2\ X\ 10^{-2}$$

$$We_L (Weber\ number\ for\ liquid) = L^2 / \sigma_L \rho_L a_v \tag{51}$$

$$3.4\ X\ 10^{-7} < We_L < 9.1\ X\ 10^{-4}$$

Wammes et al investigated the influence of pressure on liquid holdup in trickle bed reactors operating at low gas velocities. Their data fit into a correlation very much similar to that by Specchia and Baldi (1977) for liquid saturation in poor interaction regime:

$$\beta_D = 3.8(Re_L)^{0.545}(Ga^*)^{-0.42}\left(\frac{a_v D_P}{\epsilon}\right)^{0.65} \tag{52}$$

$$1.9 \; cm/s < v_g < 5.2 \; cm/s$$

The pressure drop and liquid holdup correlations listed above are the most significant ones in literature and have been widely cited. These were selected from the experimental studies listed in Table 1 based on how well they are cited in literature, and also on their relevance to this study with regard to applicability to non-foaming systems, operating conditions, and packing characteristics.

I.3. Research Motivation

Although an extensive amount of research can be found in literature on the hydrodynamics of a trickle bed reactor, there exists a historical disconnect between academic predictions and industrial data. Moreover, there is a general level of disagreement amongst correlations from different studies. This is because most of the correlations and flow maps are restricted to a limited range of experimental conditions, reactor sizes, and packing geometries specific to that used by the authors, and industrial data are needed to confirm their validity in large towers [28, 35, 36, 39, 50].

A majority of data in literature is taken in laboratory reactors, which are usually less than 20 cm in diameter and a meter in length. In other words, column-to-particle diameter (D_C/D_P) ratio encountered in literature is less than 20 in most cases, whereas commercial columns exhibit a D_C/D_P of 1000 or higher. Consequently, wall effects can significantly alter the two-phase flow hydrodynamics through the packed bed. For low D_C/D_P ratios (< 5), bed porosity is much higher near walls, while the effect decreases and becomes negligible for larger columns [3]. In addition, pressure drop measurements in small scale experiments can be inaccurate due to reactor end effects [9], resulting in deviation from the industrial operation. Therefore, more data are needed for columns with larger diameters [2].

Up until the 1970s, most correlations were based on data obtained from absorption columns that use large particles for packing [52]. Subsequently, even after the incorporation of smaller and different particle geometries like spheres, cylinders and multi-lobes, a noticeable difference in the data for different packing types can be observed from literature. For example, Charpentier and Favier [26] observed that dynamic liquid saturation is higher in case of cylindrical shaped packing as compared to spherical shaped packing. A substantial amount of data in literature is based on either spherical particles, or cylinders that are either equilateral or have a low aspect ratio. Increasing the aspect ratio reduces the particle sphericity, and can increase the deviation from the available data. Many cylindrical catalyst particles in the industry have aspect ratios higher than 5, which can result in a unique packing arrangement/orientation of the particles in the bed. The overall configuration of packing significantly affects the two-

phase flow pattern through the packing and consequently the hydrodynamic parameters, thereby impacting effective wetting, heat, and mass transfer rates [3].

This research aims to fill in the aforementioned gap in literature by publishing data collected from a very large diameter column. In addition, the packing used in the study consists of cylindrical extrudates of high aspect ratio (Length/Diameter > 5). The results are expected to provide a better insight into hydrodynamics and operation of industrial scale reactors.

This chapter covered an introduction to trickle bed reactors and the associated hydrodynamic parameters that were experimentally observed as a part of this study. Selected studies from literature were presented that proposed correlations based on experimental data and dimensionless numbers of physical significance. Chapter II describes the experimental setup and data acquisition and control in detail. Chapter III presents the experimental methodology employed, results obtained, and comparison of data with the existing correlations in literature. The last chapter summarizes the findings from this study, alongside recommendations for future research.

CHAPTER II

EXPERIMENTAL SETUP

As noted in the previous chapter, considerable experimental research can be found in literature on the study of hydrodynamic parameters of trickle bed reactors. In order to bridge the gap between academic results and industrial operation, this study aims to gather data from a large-scale column, and compare it to the existing correlations in literature. This chapter details the experimental setup that was employed and describes the data acquisition process.

II.1. Experimental Apparatus

The experimental setup consists of a 10 ft. long and 13 in. ID acrylic column filled with non-porous cylindrical shaped packing. Auxiliary equipment includes a storage tank, centrifugal pump, and the associated piping, valves and fittings. Instrumentation comprises of different sensors for measuring data, and the associated software and hardware devices for data acquisition and signal conditioning.

II.1.1. Column

The entire column is made of 0.5 in. thick acrylic and is comprised of four sections, each 13 in. ID and 14 in. OD, connected via circular flanges of 16 in. OD. Black rubber gasket (1/4 in. nominal thickness) material between each flange allows compression sealing between each section. Figure 2 is a schematic diagram of the entire structure. Following are the components of the system:

i. Top Section/Inlet: This is the top 1 ft. of the 13 in. ID column, and does not contain any packing. It has four ½ in. NPT tapped holes spaced 90° apart approximately ½ ft. from the top, for radially uniform liquid supply to the packed bed. The top flange allows attachment of a sealing cap (1/2 in. acrylic plate, 18 in. diameter) containing a single, central air inlet (via ½ in. NPT tapped hole).

ii. Packing Zone 1: The next length of 13 in. ID column is 3 ft. long, with no instrumentation or inlet/outlets installed.

iii. Packing Zone 2: The next length of 13 in. ID column is 4 ft. long, with 5 evenly spaced 0-15psig pressure transducers installed flush to the inner tube wall via ½ in. NPT-tapped holes. This enables measurement of local pressure vs. time as well as providing a multi-point measurement of pressure drop along the column.

iv. Packing Zone 3: The final length of 13 in. ID column is 2 ft. long, with an 8 in. OD (7.5 in. ID) 90° side port to facilitate loading and unloading of the packed-bed. This side port protrudes 6 in. from the vertical column and has a flange-sealed flat plate attached.

v. Outlet Zone: The outlet zone consists of 6 in. of open 13 in. ID column length with plastic skirt to minimize liquid splashing as outlet enters liquid collection drum. Between the bottom flange of packing zone 3 and the top flange of the outlet zone is a ¼ in. opening, 8-gauge stainless steel wire mesh that serves as a retaining screen for the packed bed. The top flange of this

27

zone rests on 6 evenly spaced load springs, with a slight (<1/4 in.) gap between the flange and 4 evenly spaced load cells for measuring liquid holdup.

II.1.2. Packing Material

The bottom of the column has about 2 in. height packed with ½ in. OD acrylic spheres, followed by an additional 2 in. height of ¼ in. OD acrylic spheres. These two layers prevent the actual bed packing materials (1/16 in. OD extrudates of length ¼ - ½ in.) from slipping through the retaining screen/wire mesh and clogging the pump. On top of the pre-packing layer, approximately 8-9 ft. of 1/16 in. OD extrudates are dumped to form the final packed-bed.

The packed bed has an average porosity (ε) of 46%. Equivalent particle diameter (D_P), which is the diameter of a sphere with the same volume/surface area ratio as the cylindrical packing particle, is calculated to be about 0.0022 m, or 0.087 in. The column-to-particle diameter (D_C/D_P) for the system, therefore, is about 150. This is much higher than what is frequently encountered in literature (D_C/D_P <20), and essentially closer to that of commercial reactors.

II.1.3. Air Line

Dry air is supplied from house air header at a supply pressure of 110 psig, through a ½ in. copper line containing a ball valve (yellow handle) for rapid shut-off of air pressure to the experiment. This is let down to a delivery pressure of 10 psig by a secondary pressure regulator, followed by a manually controlled gate valve. A 0 – 400 SLPM digital mass flow controller provides computer-controlled supply of air to the

column. An adjustable back-pressure regulator (set to 7.5 psig relief pressure) is located downstream of the flow controller to allow venting to atmosphere of excess air to prevent column overpressure. The gas inlet to the column has a check valve that prevents any backflow of liquid from the distributor column. Downstream of the check valve, is a pressure transducer to measure the bed top pressure, and a pressure safety valve that is set at 15 psig in case all safety measures from upstream fail to protect the equipment from overpressure.

II.1.4. Liquid Line

Water is stored in a 135-gallon steel tank, and is recirculated via a 7.5 HP centrifugal pump (with an impeller diameter of 13 in. rotating at 3500 RPM). The liquid line is equipped with an electronically actuated ball valve controlled by computer and a self-powered paddle-wheel flow meter, located downstream of the ball valve. Signal from the paddle-wheel is hardware conditioned and converted to constant-magnitude amplified square wave, before being sent to computer, which translates approximately one second of continuous data to a single frequency value for calculating liquid flow.
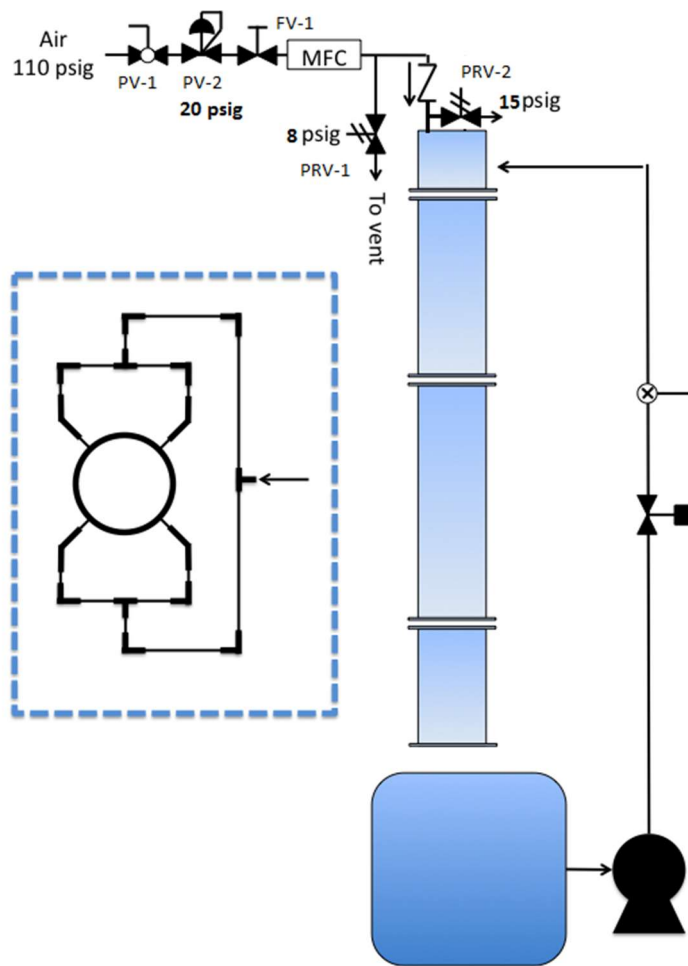
Figure 2. Schematic of experimental apparatus, showing four interchangeable column zones, liquid recirculation line and gas line; (inset) top-down illustration of 4-point liquid inlet to inlet/distributor zone

II.2. Data Acquisition/Control

The data from the system follow the path as shown in Figure 3. Fluid flow rates, pressure readings, and liquid load measurement, are all measured using respective sensor instruments. The output (analog signal) is sent to a signal collection box, which acts as a junction between sensors and the data acquisition device. Here, a 9VDC power is

supplied in order to amplify the signal from the sensor, and 12-guage wires carry the signals to the separate input channels in the data acquisition device. The device is plugged into the computer, in which the signals are processed, conditioned and converted to readable data using LabView software.
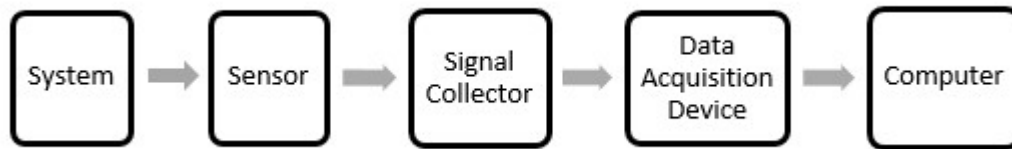

Figure 3. Data acquisition

II.2.1. Sensors

An array of sensors was employed to measure liquid and gas flow rates, and local pressures and overall liquid holdup in the column. Raw signal from each sensor is converted to the final value after signal conditioning and sensor calibration. Following sensors were used to record the data from the system:

i. *Load Sensors*

Four load sensors have been used to measure the mass of liquid held in the column at any given point of time. This is used for the calculation of dynamic liquid saturation corresponding to the existing operating conditions. These sensors consist of a metal housing containing a flexible membrane with Wheatstone bridge circuit patterned on it. At zero load, the bridge is balanced, and application of input voltage does not give any output signal voltage. As some load is applied, the bridge becomes unbalanced, and

application of an input voltage creates an output voltage. The amplitude of this raw

output signal, after the required signal conditioning, is translated using manufacturer-

supplied calibration factor, to obtain the total additional load M (kg) in the column. This

is converted to dynamic liquid saturation as follows:

$$\beta_D(\%) = \frac{M\rho_L}{(\pi D_P^2 H)\epsilon}$$

ii.   *Pressure Transducers*

Four pressure transducers are installed at different locations in the column – one

is inserted at the top, while three are inserted in the middle of the packing at some

distance from each other. These transducers too are based on Wheatstone bridge as

described in case of load sensors. The amplitude of the raw output signal, after the

required signal conditioning, is translated using manufacturer-supplied calibration factor,

to obtain the local pressure reading (psig) in the column. The pressure readings at

different portions of the column are used to arrive at the pressure drop per unit length

(psi/ft) at the existing operating conditions.

iii.   *Liquid Flow Meter*

Liquid flow is measured using a self-powered paddlewheel type flow meter,

which is inserted into the liquid piping about 5 ft downstream of the flow control valve.

The 4-paddle free spinning wheel at the end of the flow meter (Figure 4) rotates at a

speed proportional to the flow velocity.

The flow meter output is a raw signal that is passed through a comparator/

operational amplifier circuit that converts it into a fixed magnitude (9V) square wave.

Frequency of this conditioned signal is measured using Fourier Transform in LabView, which is then converted to the corresponding flow rate using a calibration factor.
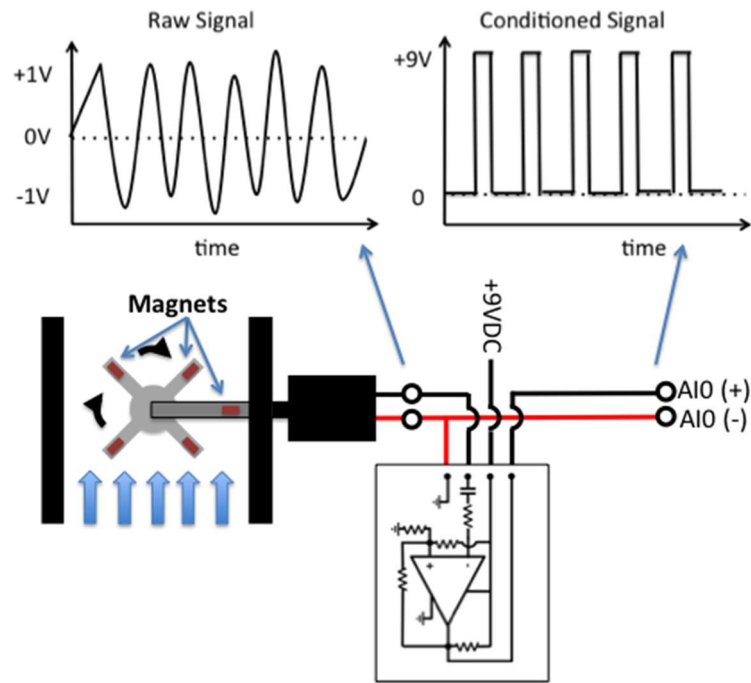

Figure 4. Paddle-wheel flow meter for measuring liquid flow rate

iv.   *Gas Mass Flow Controller*

Air flow is measured as well as controlled by a single Mass Flow Controller (MFC) instrument installed in the air line upstream of the inlet to column. The maximum capacity of the MFC is 400 SLPM of gas flow.

II.2.2. Computer Control via LabView

LabView software is used to manage all data acquisition from the pressure and load sensors. In normal operation, it is programmed to sample 1s worth of data, at a rate

of 100 data points per second (i.e., 100 Hz). Once steady-state is reached, it is switched to 'Record Mode', where two minutes of data are recorded in an excel sheet, again at a rate of 100 data samples per second, totaling 12000 data points spread over two minutes. The data are averaged to obtain the single value of pressure and liquid holdup at steady state operation, along with the standard deviation over the two minute interval.

In addition, liquid flow is controlled via an electronically actuated ball valve controlled by LabView on computer. A closed-loop feedback control strategy is used in which the user-input set point is compared with the operating point (liquid flow rate, gpm). After sampling the flow rate, the computer sends a control signal 'pulse' of duration 0.1s to the ball valve to adjust the flow rate till the set point matches the operating point. The LabView software includes a manual override button, which allows the user to disconnect the closed-loop flow control in favor of manual control of the ball valve; each click on the ball valve controls sends a 0.1s pulse or incremental adjustment of the ball valve. The pulse-wise control of the ball valve allows the user (or computer control) to re-assess liquid flow before another adjustment, therefore avoiding over-control and flooding of the column.

In summary, this chapter covered an overview of the experimental setup, with a detailed description of each equipment and instrument that was integral to the operation, data measurement and acquisition, and safety of the system. Chapter III presents the methodology followed to gather data, results obtained, and comparison with existing knowledge in literature.

CHAPTER III

RESULTS AND DISCUSSION

Trickle bed reactors are one of the most commonly used industrial reactors for carrying out reactions of gas and liquid phase reactants on a solid catalyst packing. Hydrodynamics of such reactors continues to be a focus area due to the complexities associated with multi-phase flow. The objective of this study is to bridge the gap between laboratory and industrial scale operation by gathering data from a large scale column, and to supplement research on hydrodynamics in the low gas superficial velocity range. In Chapter I, key hydrodynamic parameters in trickle bed reactors are described, along with the available knowledge that can be employed for their prediction to aid in reactor design and performance evaluation. Chapter II describes the experimental setup that was employed to collect data that can provide better insight into the industrial scale of operations. This Chapter presents the hydrodynamic data collected and analyzed with respect to existing correlations in literature. Observations made with respect to flow regime transition at the operating conditions studied are also presented.

III.1. Operation

Data were collected for the following operating range, analyzed for trends and compared with the existing knowledge based on previously done experimental work on Trickle Bed Reactors.

✓ Gas Flow (G) = 5 to 400 SLPM (G' = 0.001 to 0.1 $kg/m^2/s$)

✓ Liquid Flow (L) = 6 to 60 gpm (L' = 4.4 to 44 $kg/m^2/s$)

In each case, the gas flow rate was fixed at some value, while the liquid flow rate was increased incrementally. To visualize the operational range covered by our experimental work, existing flow maps were used, as developed by Sato et al, 1973 [25] and Charpentier and Favier, 1975 [26]. The region of interest is highlighted in the flow maps shown in Figure 5 (a) and (b). The operating conditions correspond to a very low gas to liquid ratio, quite common in the industry but rarely encountered in literature. Here, a major part of the range lies in the low interaction regime, and touches the pulsing flow regime and the bubble flow regime at various portions of the map.
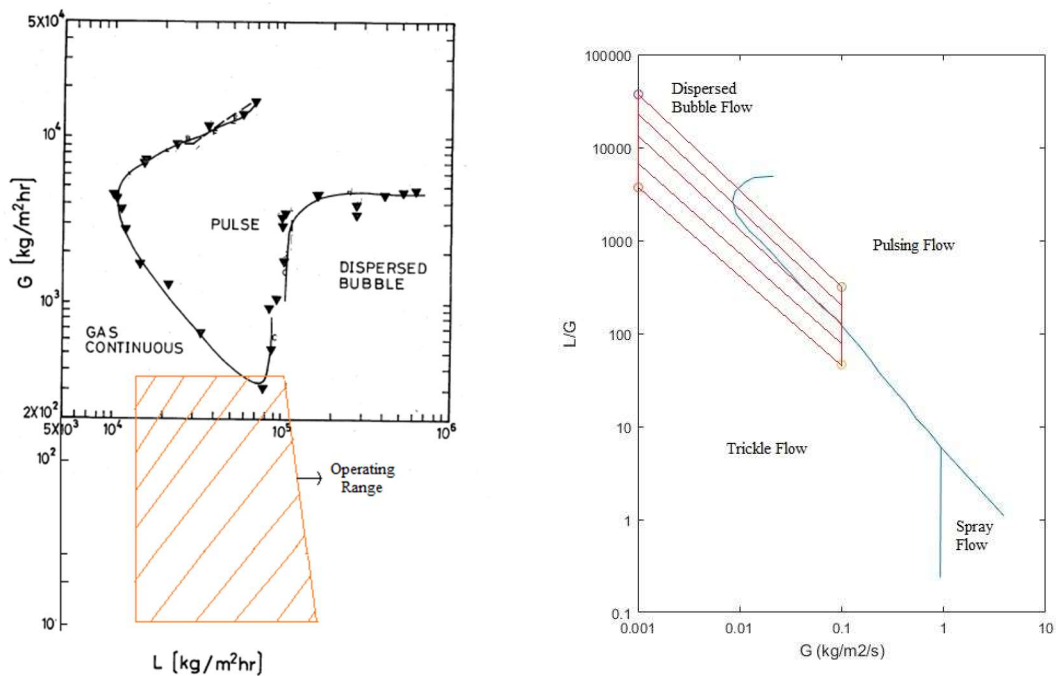
Figure 5. Flow maps depicting the operating range in this study (a) Flow map by Sato et al [25] (b) Flow map by Charpentier et al [26]

36

At every experimental run, hydrodynamic data were extracted from the system when there was a negligible change in the data from the previous two consecutive trials. For most runs, steady state is achieved at an approximate interval of 10 to 15 minutes after operating variables are changed. Liquid saturation was calculated from the load cell readings, and pressure drop was calculated from pressure transducer readings. While local variations in liquid load and pressure drop across the column are expected, the hydrodynamic data taken in all experimental runs is assumed to be the average value for the column.

Flow is relatively undeveloped in the top 20-30% of the column (as observed visually) due to incomplete mixing of the two fluids, and pressure transducers were inserted in the bottom half of the column (except for one installed at the top) to have more accuracy in local pressure measurement. Pressure drop was calculated between each of the pressure transducers, and it was observed that the resulting values did not differ by a significant margin from each other. The final pressure drop reported in the study is the average of all pressure drop values calculated across each transducer.

Hysteresis was exhibited by the system, as observed from the liquid holdup and pressure drop values, mainly at the lower liquid flow values. This observation is also reported by many authors [19, 35, 40]. Figure 6 shows the hysteresis observed at a gas flow rate of 100 SLPM. At increasing liquid flow, liquid flows down in the form of channeled rivulets through the relatively dry packing. As the flow is increased, it begins spread to other portions of the packing that were previously not in contact with the liquid. Once the liquid flow is high enough, a substantial portion of the packing now gets

covered in a thin film of liquid with liquid bridges between the packing that need to be broken down by the gas flow. Therefore, as the liquid flow is now decreased, the gas encounters higher pressure drop than in the case when the liquid flow was being increased. At the same time, a more uniformly wetted packing sees a comparatively higher value of liquid holdup.

In order to obtain consistent readings that are more representative of the industrial columns, the packing was subjected to a high interaction regime (high liquid and gas flows) before bringing down the flow rates to the set points. This pre-wetting procedure is commonly followed by many authors in literature [38, 40].
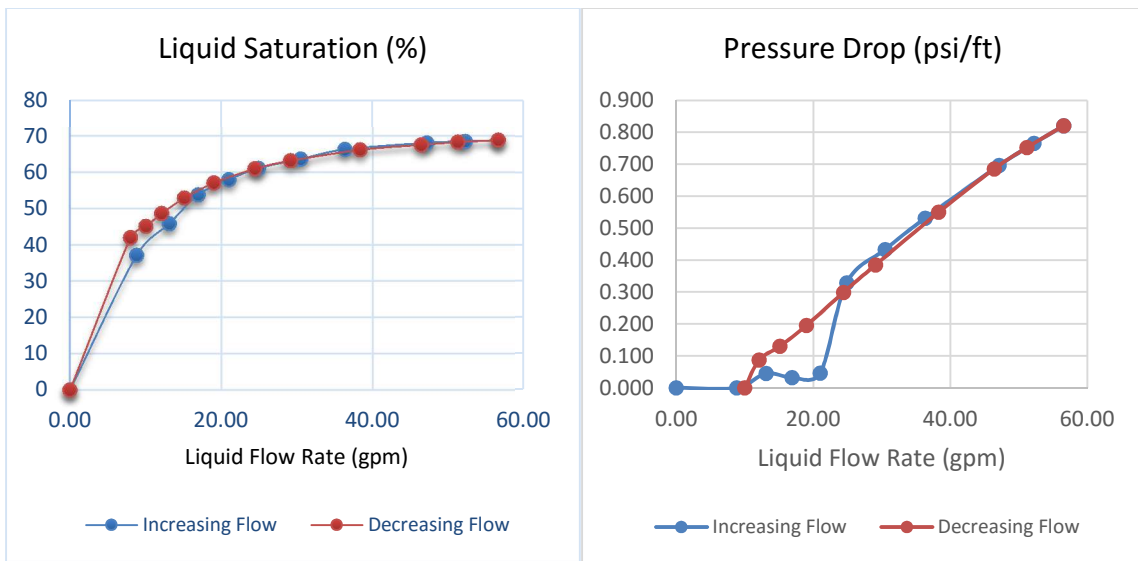
Figure 6. Hysteresis observed in liquid holdup and pressure drop readings

III.2. Pressure Drop

As described in Section I.2.2, pressure drop is an important parameter in design of commercial reactors. Larger reactors can have different pressure drop behavior from laboratory scale reactors, due to negligible wall effects and reduction in fluid density along the bed length. Pressure drop estimation is useful in predicting feed pressure, since many reactors operate at a constant feed pressure. In addition, it is a key parameter in estimation of heat and mass transfer coefficients. The following subsections detail the pressure drop trend recorded at the aforementioned operating conditions and how it compares to the prediction by existing correlations.

III.2.1. Pressure Drop Data

The pressure drop data obtained for the trickle bed column are shown in Figure 7. At most gas flow rates, the frictional pressure drop remains zero for liquid flow rates up to around 15 gpm, and liquid flow is gravity driven. At higher liquid flows, liquid spreads radially while flowing down through the packing, and drag forces between the two phases come into play, which increases the pressure drop with increasing liquid flow. At higher gas flow rates, the gravity drainage portion becomes less significant, because of some level of gas-liquid interaction even at low liquid flow rates. Figure 7 shows plots with two sets of experimental data each, arbitrarily paired for the purpose of comparison. As can be seen, at the low gas velocities range in which our entire operational lies (0-70 cm/s), there is not a significant difference in pressure drop values as the gas flow rate is increased, and the pressure drop trend is quite similar at all gas flow rates.
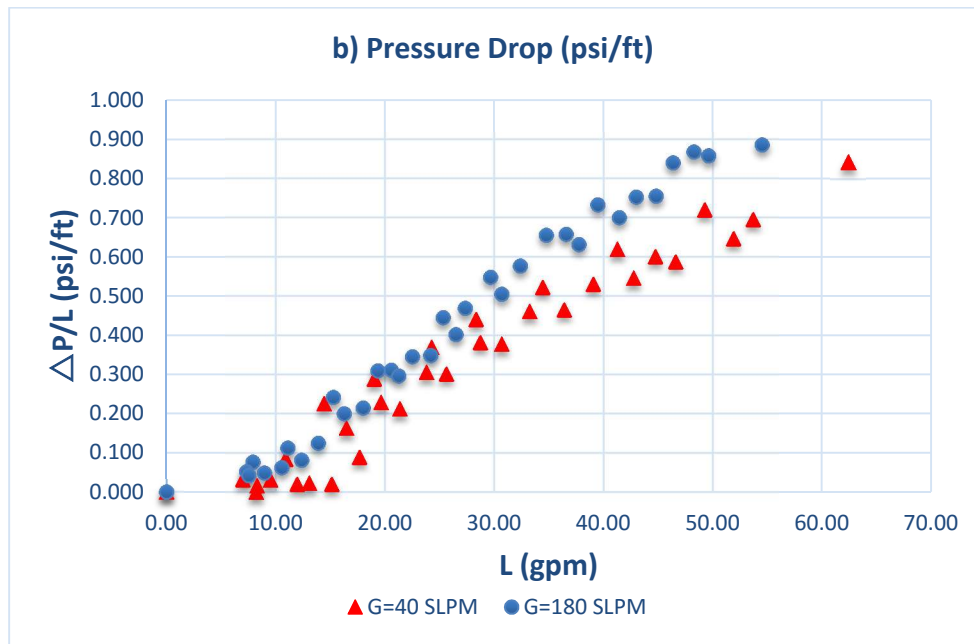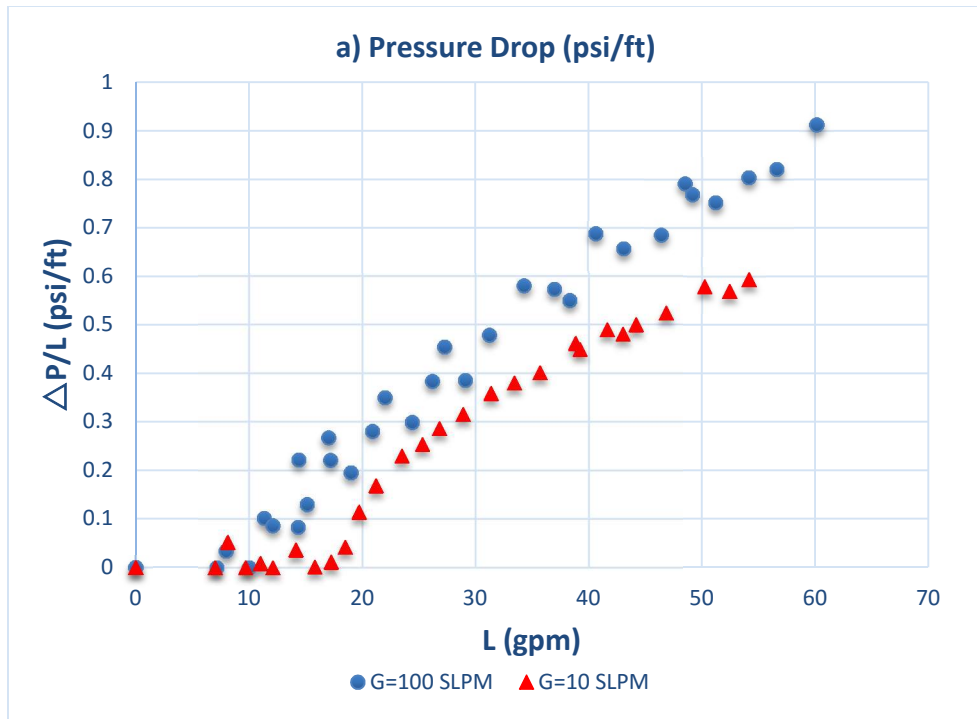
Figure 7. Experimental data representing pressure drop for a) G = 10 and 100 SLPM, b) G = 40 and 180 SLPM, c) 80 and 220 SLPM, d) 120 and 300 SLPM, and e) 160 and 400 SLPM
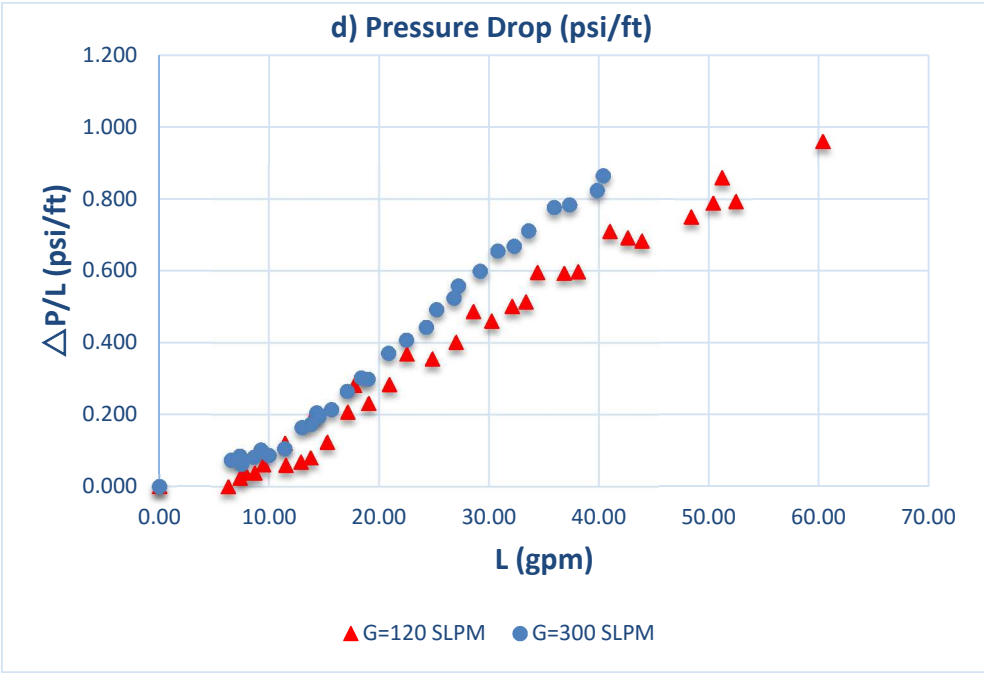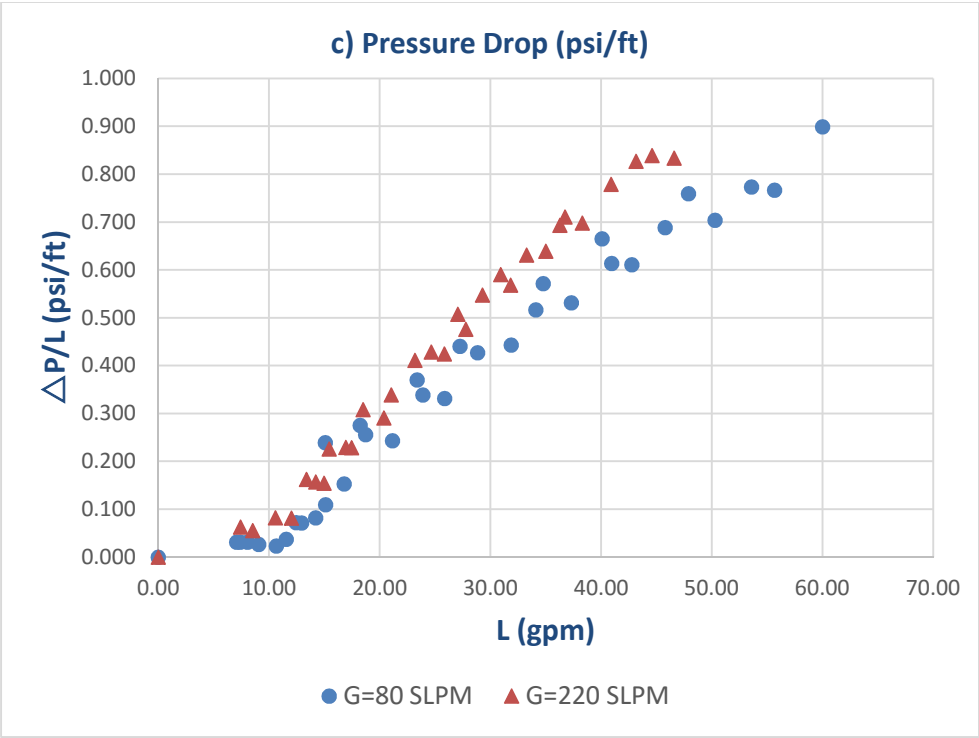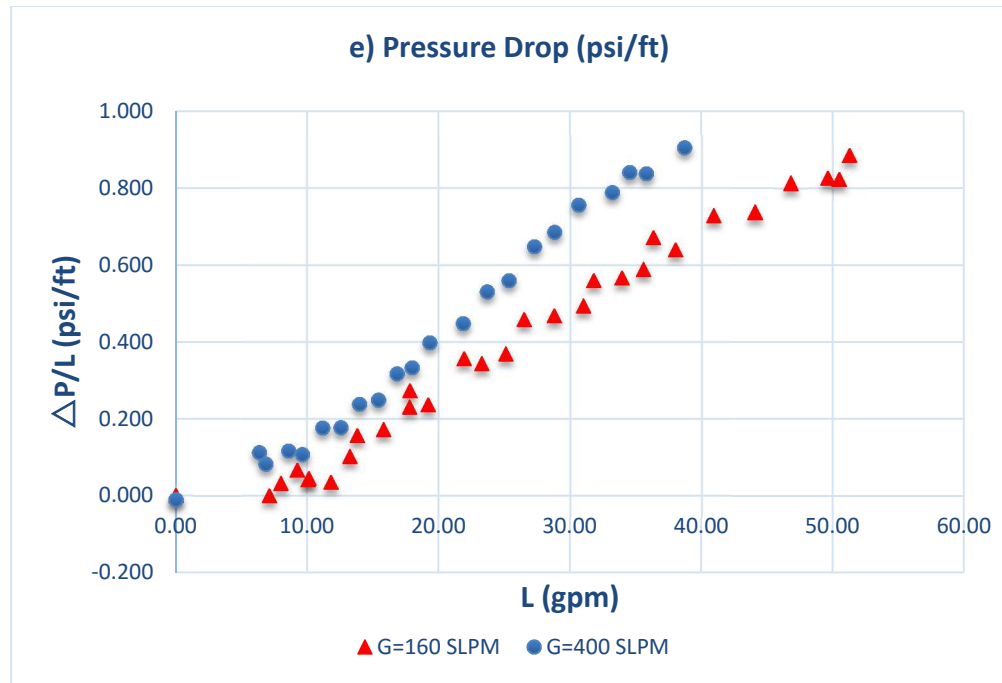
40

Figure 7 Continued.

Figure 7 Continued.

III.2.2. Comparison with Literature

Data obtained were compared with correlations listed in Chapter I to check which set of correlations give the closest estimate. Some of those correlations have been selected based on their wide use and citations by other authors, and are plotted below.

For the purpose of comparison, data for only two gas flow rates, 80 SLPM (Figure 8) and 300 SLPM (Figure 9), are plotted along with the trend predicted by various correlations. It was observed that many of the correlations do not agree with each other, and also do not give a close prediction of the data. Figure 10 shows parity plots of selected pressure drop correlations that give the closest estimate to the experimental data, against more than 300 data points.
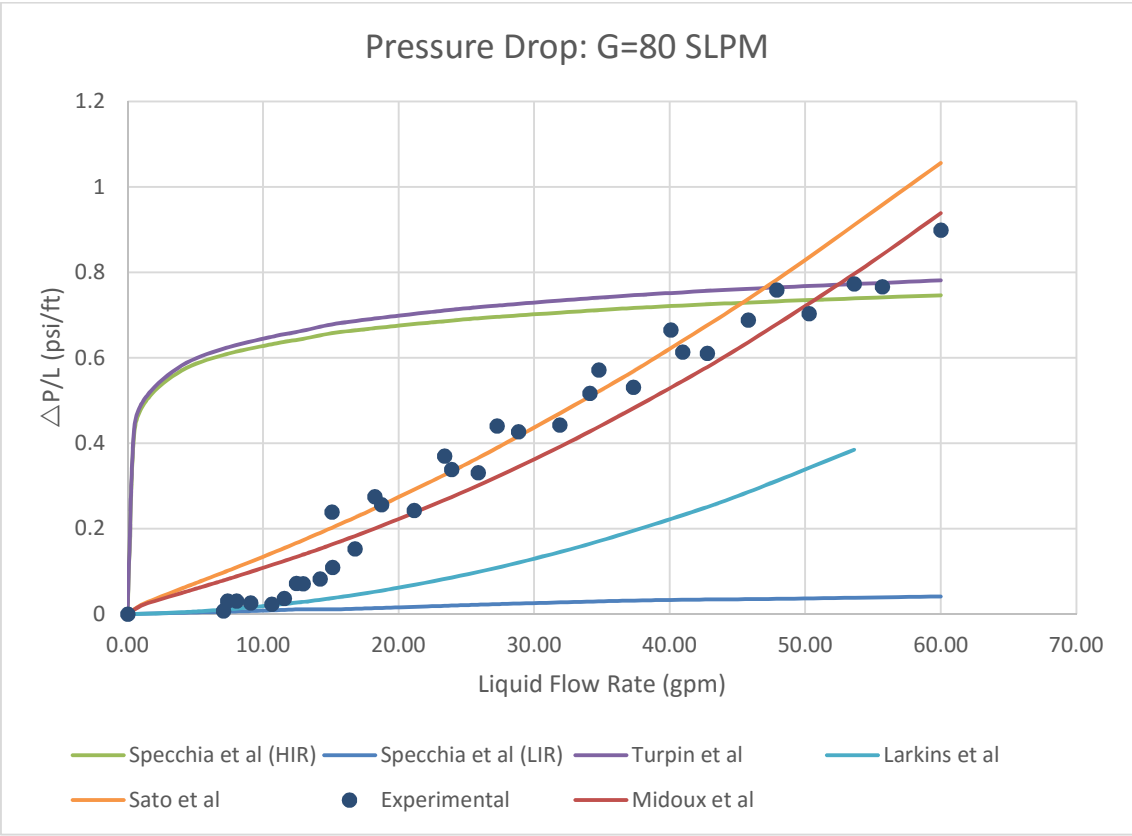
Figure 8. Pressure drop data for G = 80 SLPM compared to existing correlations
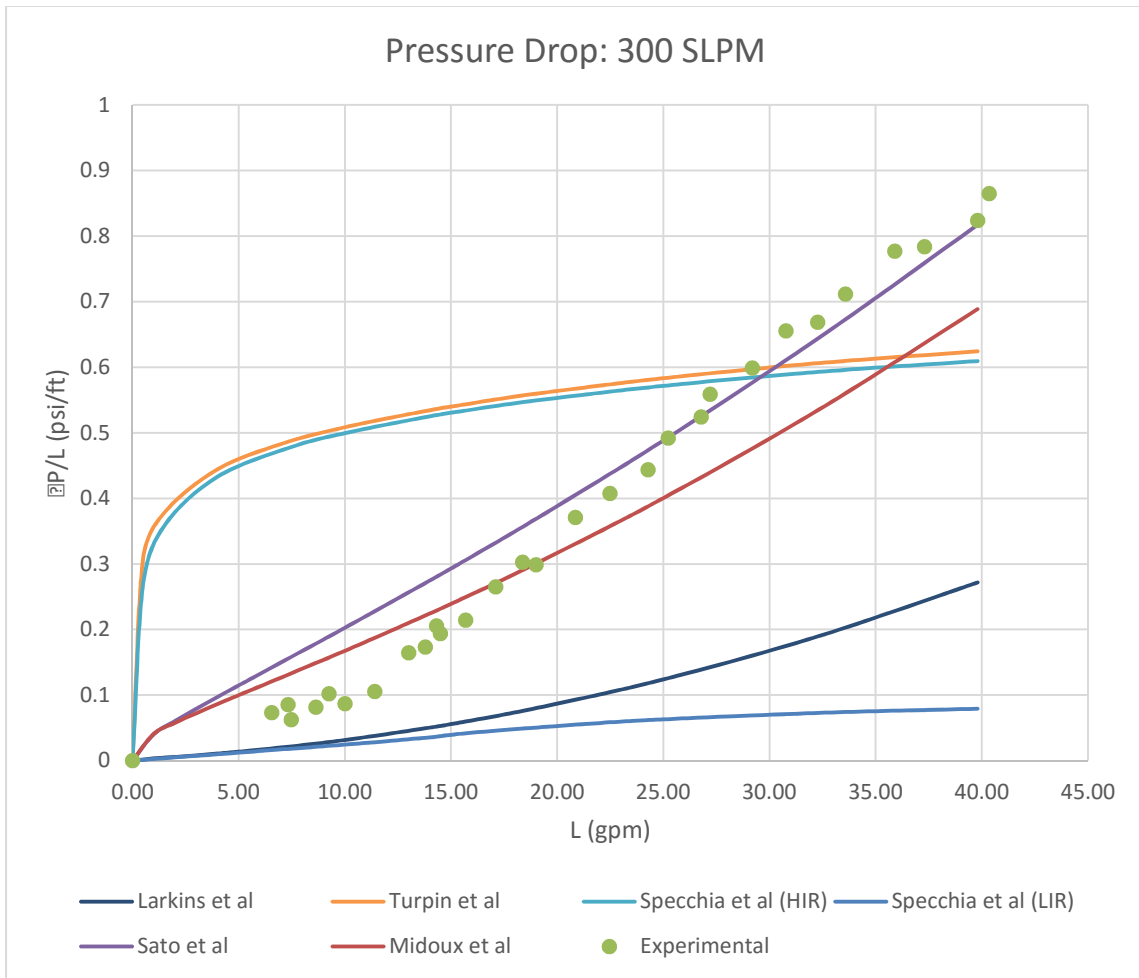
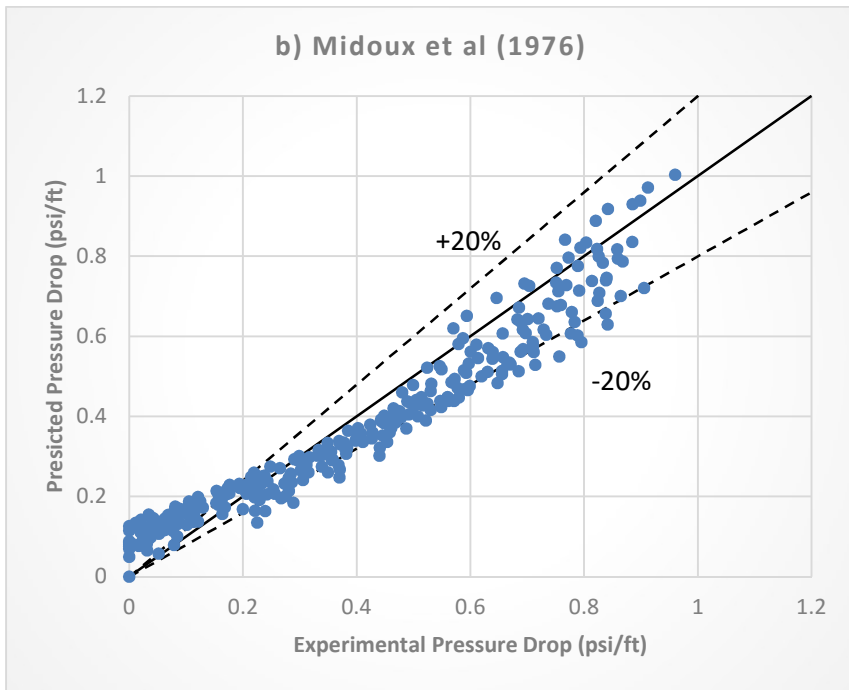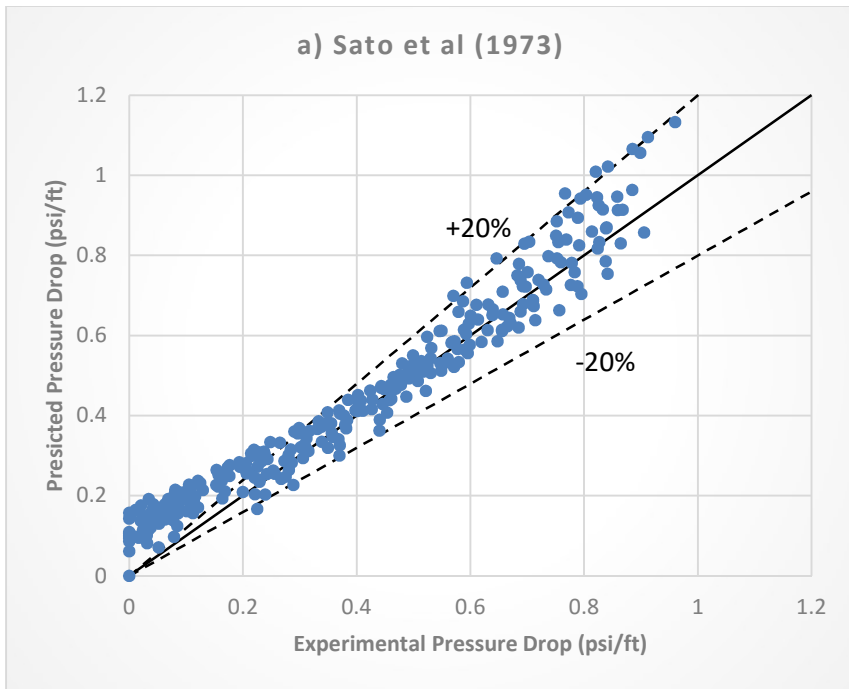**Figure 9.** Pressure drop data for G = 300 SLPM compared to existing correlations

Figure 10. Parity plots for pressure drop correlations by (a) Sato et al (1973) (b) Midoux et al (1976)

Some observations that can be made from the comparison of pressure drop data to the tested correlations, are:

i. These correlations do not account for gravity drainage, which is significant at low liquid flow rates, especially in the low gas velocity regime specific to the operating range in this study. The driving force for liquid flow comprises of the gravitational flow and the drag force between the gas and liquid [37]. At liquid flow rates up to 10 – 15 gpm, drag forces are negligible due to a very low interaction between the two fluids, and the liquid flowing mostly due to gravitational force. At this time, the recorded frictional pressure drop in the bed is approximately zero, and the conditions resemble a single-liquid trickle flow experiment [18, 28, 37]. As liquid flow is increased, liquid spreads over to other regions in the packing, wetting it more uniformly. Therefore, drag forces come become significant, increasing the frictional pressure drop reading in the column. Most correlations in literature have been tested at much higher gas velocities (even for 'Low Interaction Regime' or trickle flow regime), and thus represent a different realm of hydrodynamics than what is observed at low gas velocities.

ii. Correlation proposed by Sato et al (1973), and by Midoux et al (1976), give the closest estimate for the entire operational regime studied, again with significant deviation at lower liquid flow rates due to strong gravity assisted drainage. At higher liquid flows, data fall within $\pm 20\%$ range of the prediction.

iii.   All other correlations show a trend significantly dissimilar from the collected data, and from each other as well.

iv.   Categorizing the pressure drop correlations into High and Low Interaction regimes (i.e., pulsing and trickling flow, respectively) may not be representative of every range of operation, especially that of operation at low gas velocities. The correlations by Specchia and Baldi [28] thus do not satisfy the data.

III.3. Liquid Saturation

As mentioned in Section I.2.3, static liquid holdup is represented by the Eötvös number, which can be calculated for our system as:

$$E\ddot{o} = \frac{\rho_l g D_P^2}{\sigma_l} = 0.65$$

From Figure 11 published by Swaaij et al, 1969 [53], it can be seen that for $E\ddot{o} < 5$, value of $\epsilon\beta_S$ is about 0.05. This gives

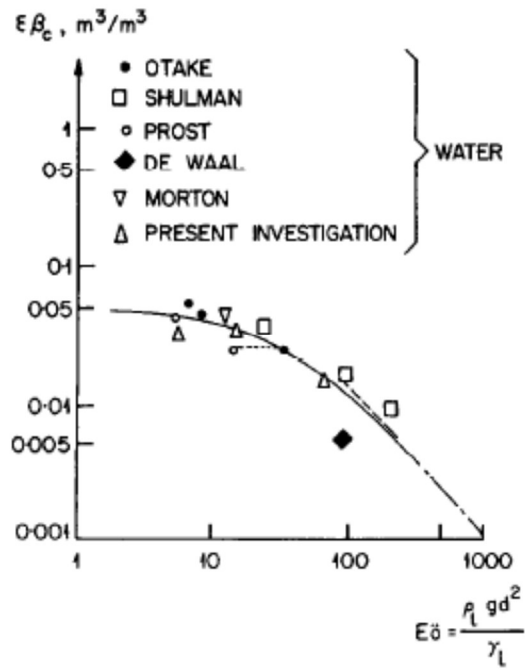$$\epsilon\beta_S = 0.05$$

$$\beta_S \sim 11\%$$

Figure 11. Correlation of static liquid holdup with Eötvös number [53]

Therefore, static saturation for the column in our system can be taken as 11%. The load sensors used in our system give a measurement of the dynamic saturation, which is also predicted by a majority of correlations in literature. For the correlations that predict the total liquid saturation [18, 24, 27], the static liquid saturation can be deducted to arrive at the dynamic saturation. The following subsections detail the liquid saturation trend recorded at the aforementioned operating conditions and how it compares to the prediction by existing correlations.

III.3.1. Liquid Saturation Data

The liquid saturation data for the Trickle Bed column were collected and are represented by Figure 12. As previously reported in literature [1, 18, 37, 54], liquid holdup at low gas velocities is not significantly affected by increasing the gas flow.
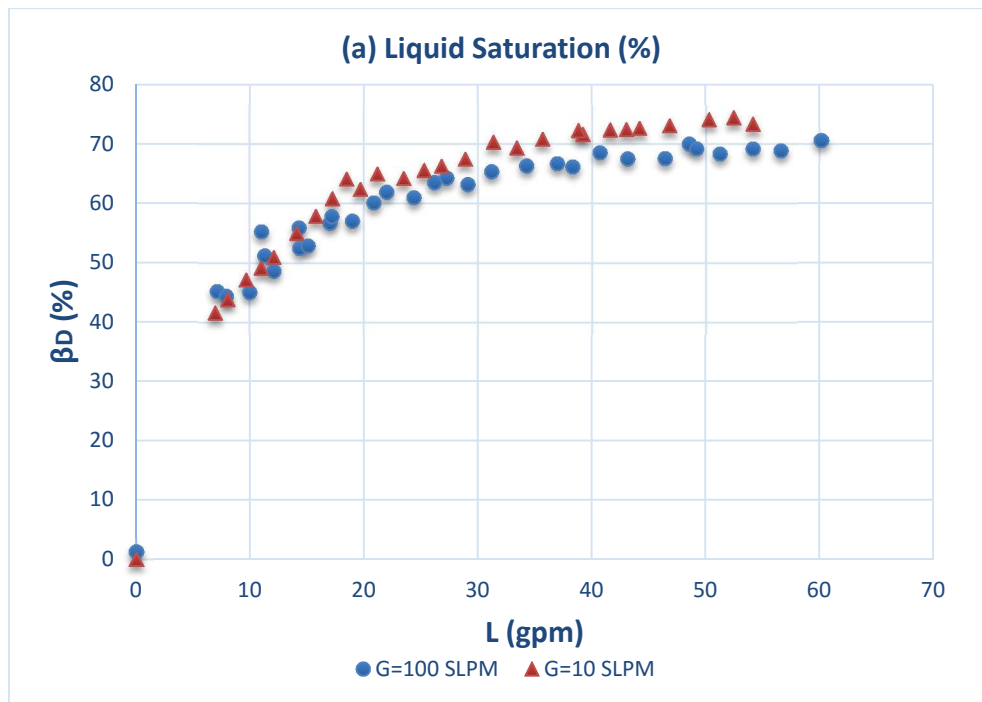
(a) Liquid Saturation (%)

Figure 12. Experimental data representing liquid saturation for a) G = 10 and 100 SLPM, b) G = 40 and 180 SLPM, c) 80 and 220 SLPM, d) 120 and 300 SLPM, and e) 160 and 400 SLPM
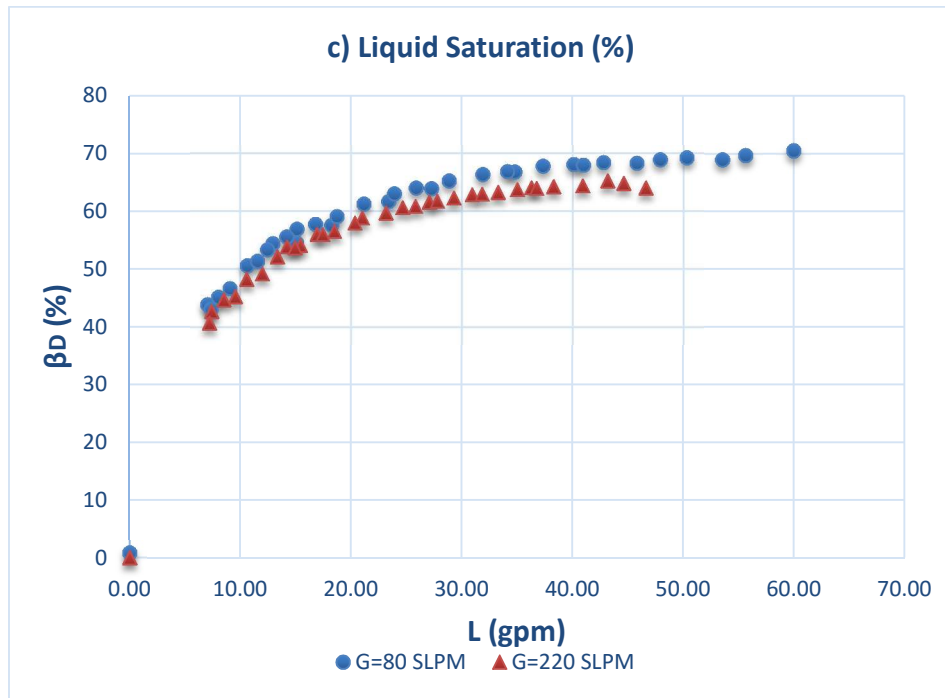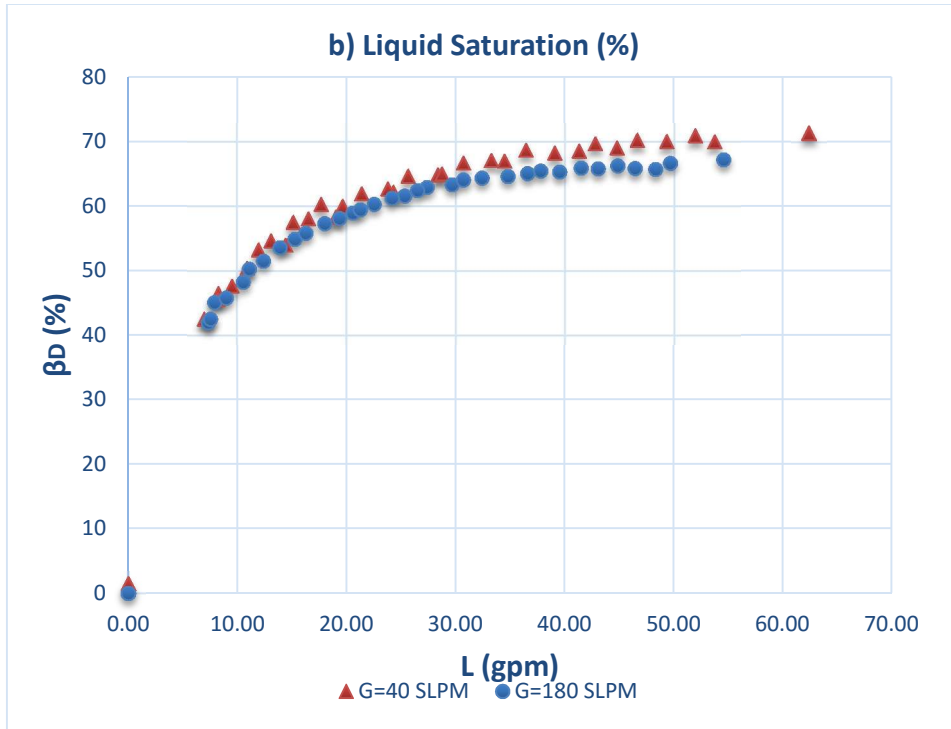
b) Liquid Saturation (%)

c) Liquid Saturation (%)

Figure 12 Continued.

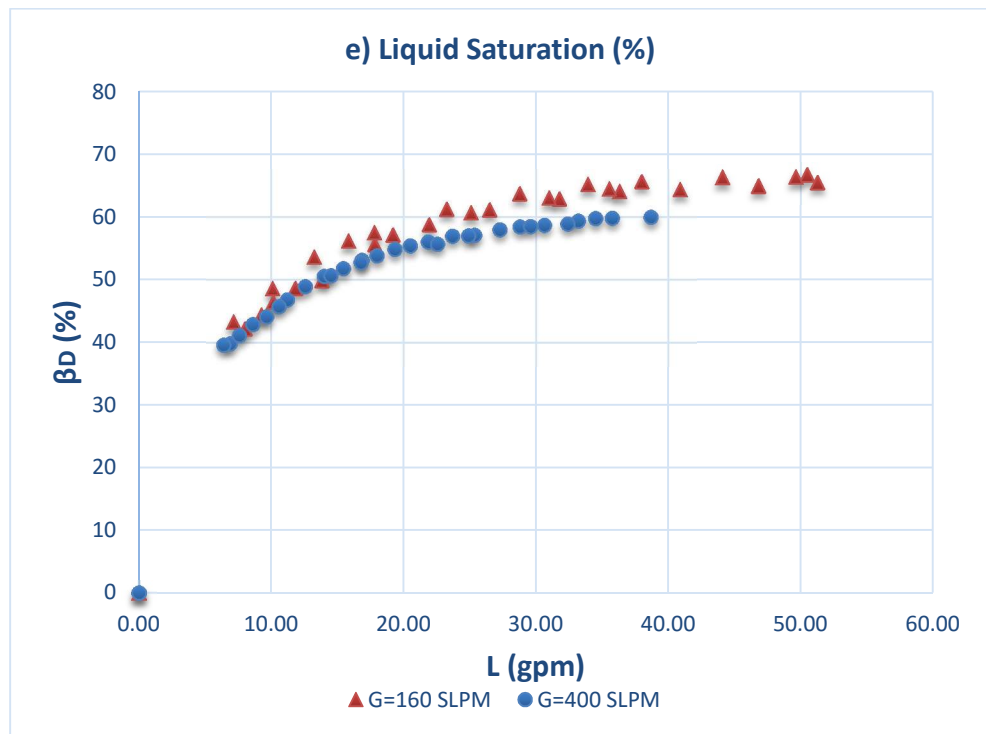d) Liquid Saturation (%)

e) Liquid Saturation (%)
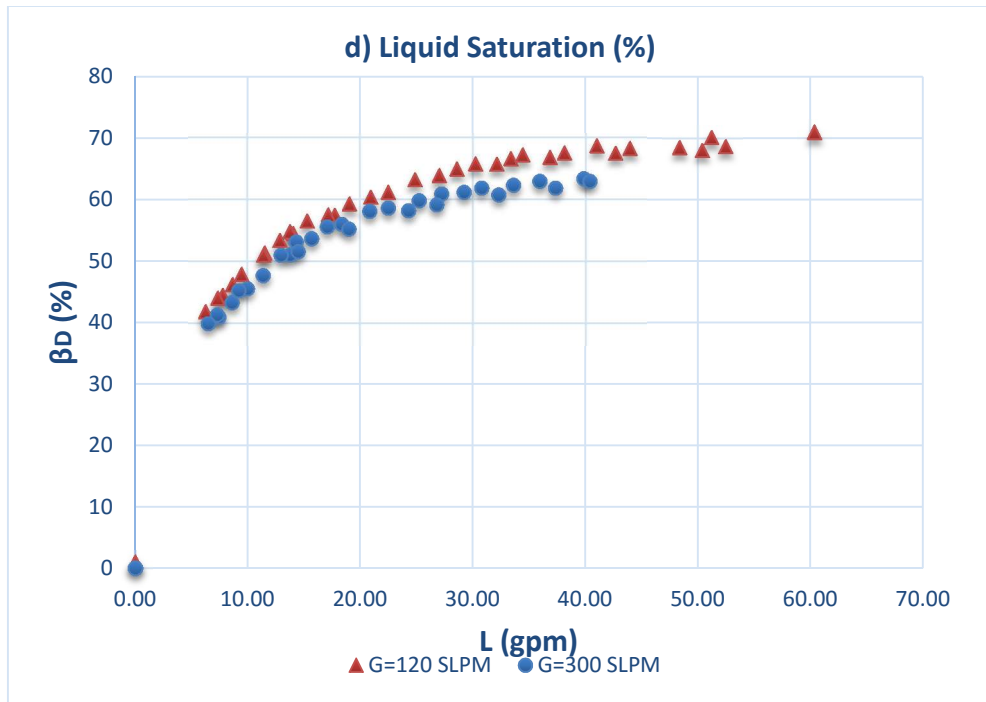
Figure 12 Continued.

III.3.2. Comparison with literature

Liquid saturation data were compared with correlations listed in Chapter I to check which set of correlations give the closest estimate. For the purpose of comparison, data for only two gas flow rates, 80 SLPM and 300 SLPM, are plotted along with the trend predicted by selected correlations (Figure 13 and Figure 14). Again, a significant disagreement between these correlations can be observed, with a few of them giving a close estimate. Figure 15 shows parity plots of the closest selected liquid saturation correlations in comparison to the experimental data representing over 300 data points.

Figure 13. Liquid saturation data for G = 80 SLPM compared to existing correlations

Figure 14. Liquid saturation data for G = 300 SLPM compared to existing correlations
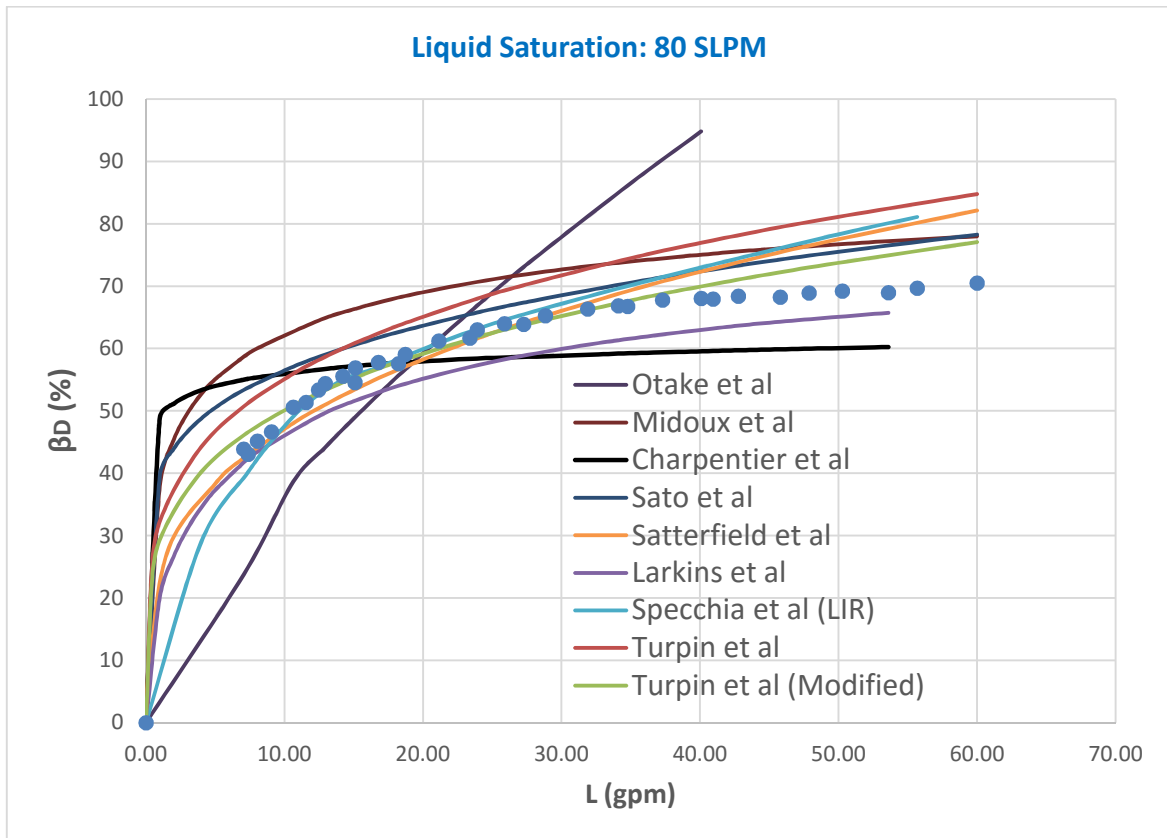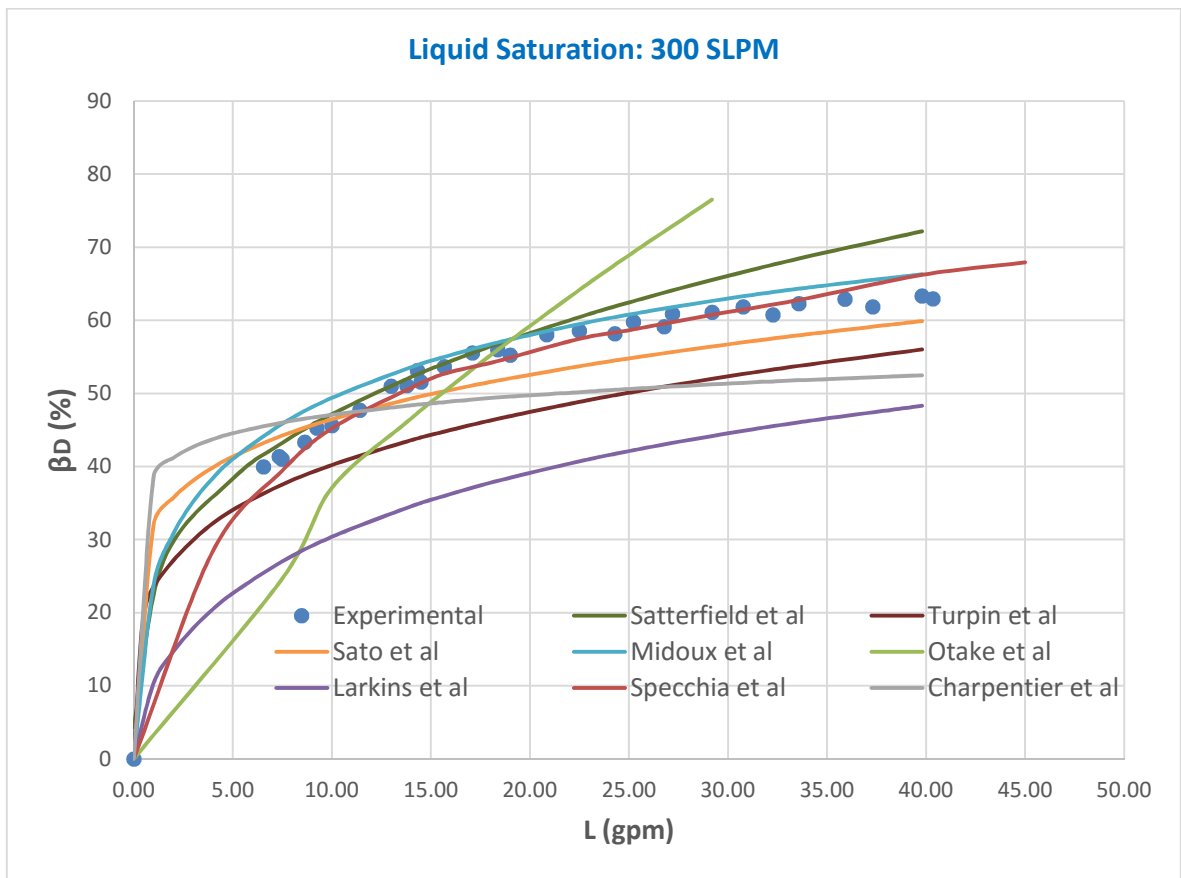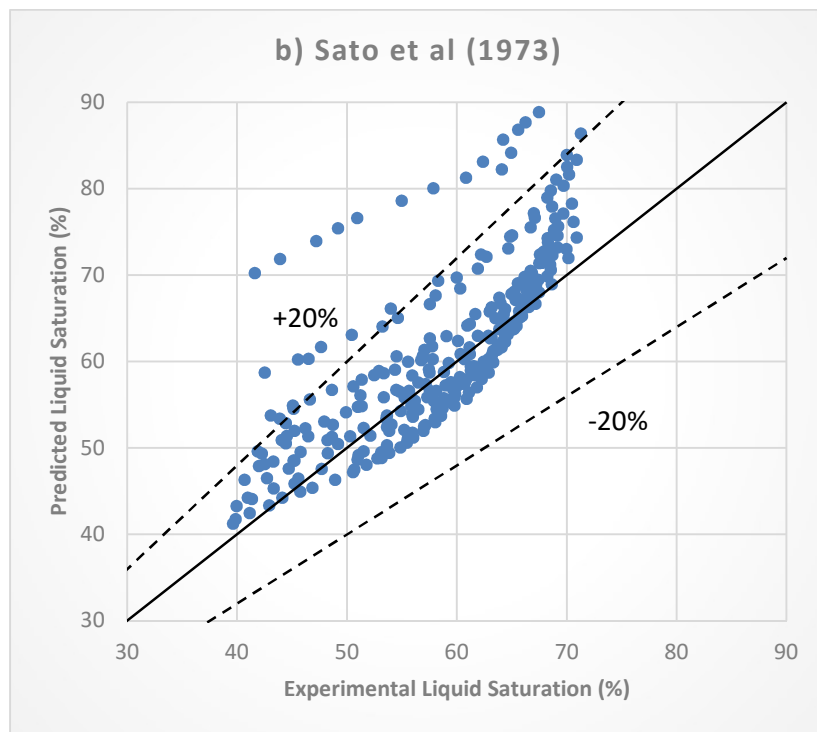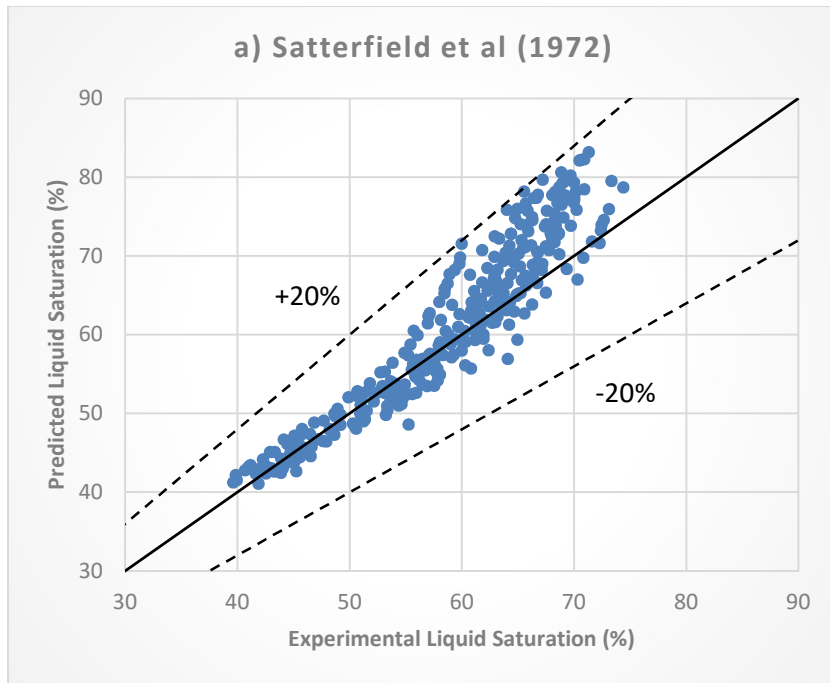
Figure 15. Parity plots for correlations by (a) Satterfield et al (1972), (b) Sato et al (1973), (c) Midoux et al (1976), and (d) Specchia et al (1977)
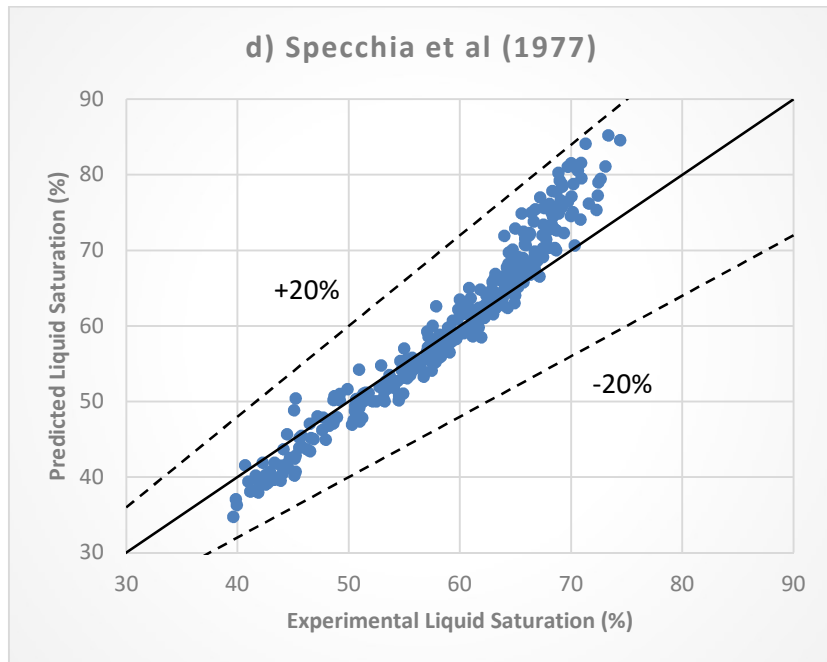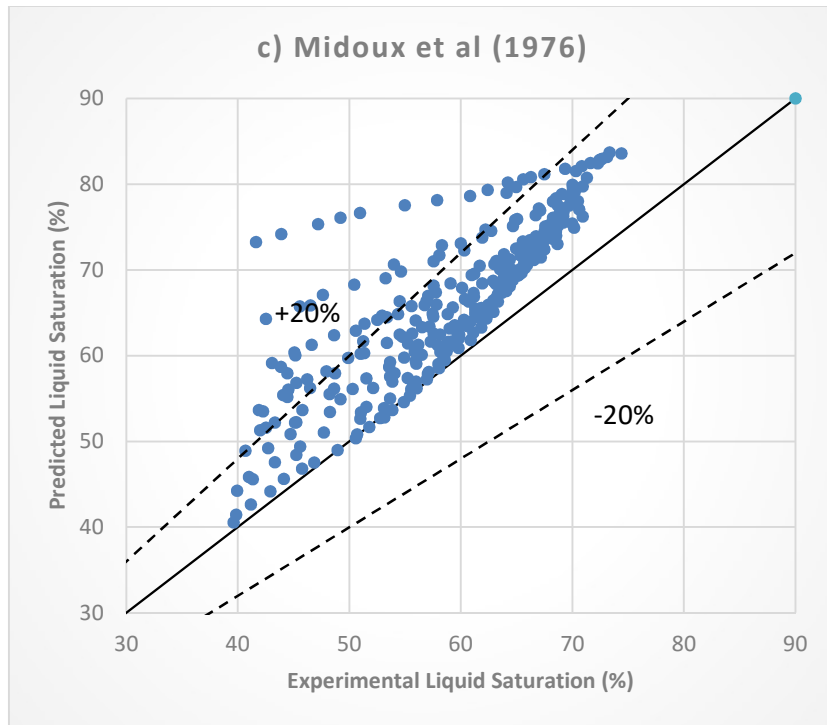
Figure 15 Continued.

55

Some observations made pertaining to the comparison of liquid holdup data with the tested correlations, are mentioned below:

i.   Correlation proposed by Turpin et al [23] is entirely empirical in nature, but gives an accurate description of the liquid saturation trend if its constants are modified. However, those constants need to be changed to different values for different gas flow rates, indicating that the correlation should also contain other factors representing the packing characteristics, fluid properties, and drag forces that result due to a higher gas flow.

ii.   Correlations proposed by Specchia and Baldi [28] for Low Interaction Regime, and a similar one proposed by Wammes et al [37], give the closest estimate in the operational regime studied, with a mean deviation of only about 6% from the experimental data, and the entire data lie in the $\pm20\%$ range of the prediction. This is due to introduction of the modified Galileo number that incorporates drag forces due to the gas flow, in addition to gravitational force on the liquid.

iii.   Correlations proposed by Satterfield et al [18], which is based on single-liquid phase trickling flow, appears to give an close prediction of liquid saturation, with a mean deviation of around 7.5% from the experimental data, with the entire data lying within $\pm20\%$ of the prediction. Since the expression does not feature gas flow, it predicts the same trend for all the gas flow rates in the low gas velocity range. This is a good approximation because for gas flow rates from 0 to 400 SLPM, the liquid saturation values only vary by a

56

maximum of 14%. However, this correlation should be used with caution for other operating ranges lying in the low interaction regime, as well as for different packing shapes and fluid properties.

iv.   Correlations proposed by Sato et al [24], and Midoux et al [27], both of which use the two-phase parameter χ to correlate the liquid saturation, give a reasonably close prediction, with a mean deviation of around 14.5% and 16.5%, respectively, from the experimental data. However, the spread increases at lower gas flow rates (Figure 15), due to which substantial data lie outside of the $\pm$20% range from the predictions.

v.   Other correlations studied do predict the data effectively, and are also in considerable disagreement with each other.

III.4. Flow Regime Transition

A majority of studies in literature are focused on trickle-to-pulse flow transition. Characterization of a transition from low interaction to high interaction regime is done mostly in two ways:

1) Visual Observation: A transition is noted when clear pulses can be seen moving down the column. These alternating gas and liquid rich slugs often start from the bottom of the column and move up as the liquid flow is increased.

2) Standard deviation method: The onset of fluctuations can be quantified as a rise in standard deviation of the pressure drop readings collected over an interval of 1-2 minutes [39, 40]. For example, Honda et al [40] used the relative standard deviation (σ_R) of pressure drop readings to characterize trickle-to-pulse and

trickle-to-bubble flow transition. Their work shows a steep rise in σ_R at a certain liquid flow rate, beyond which high interaction regime is assumed to be achieved, supported by visual observation. The authors quantified and presented results for trickle-to-bubble flow transition at a low fixed gas superficial velocity, and trickle-to-pulse flow transition at high fixed gas superficial velocity. The rise in fluctuations is more in the latter case than in the former case, which is expected due to overall higher fluid flow rates in the latter case.

The relative standard deviation is given by

$$\sigma_R = \frac{\sigma}{\sigma_B} - 1 \qquad (53)$$

where, σ_B is the baseline standard deviation (i.e., fluctuation at no flow condition)

Some researchers have reported a steep rise in pressure drop at the transition [25, 40], while some have observed little or no effect of flow regime transition on the pressure drop trend [31, 55]. Since results from the present study show that pressure drop trend is unaffected by flow regime transition, any correlation representing the data should not depend on the prevailing flow regime.

As seen from conventionally used flow maps in Figure 5, our operation lies in very low gas to liquid flow range. From the map, it is expected that trickle flow will be encountered for most of the flow rates, with a trickle to bubble flow transition at the lowest gas flow rates, while just touching the transition trickle flow to pulsing flow at higher gas flows (closer to 400 SLPM). Although there is significant amount of literature

on trickle-to-pulse flow regime transition, studies on trickle to dispersed bubble flow transition are scarce, with most of them demonstrating only a visual observation of such transition [40].

To test the applicability of the existing flow maps to our system, careful visual observation, combined with monitoring of the pressure drop and standard deviation data, was done in order to identify a transition, if any, from low interaction (trickle flow) regime to a high interaction (pulsing/bubble flow) regime.

i. *Lowest gas flow rates: G < 40 SLPM (v_G < 7 mm/s)*

Trickle flow to bubble flow transition could be observed taking place at an intermediate liquid flow rate. Other studies in literature too report trickle to dispersed-bubble flow transition only at very low gas flow rates (G'<0.01 kg/m^{2}s, or v_G < 7 mm/s) [20]. The transition was observed to be gradual rather than abrupt, and did not create substantial fluctuations in the pressure drop. At low liquid flow rates, liquid could be observed trickling down the packing in the form of thin films and rivulets, wherein some fraction of the packing remains unwetted. The relative standard deviation (σ_R) remained close to zero (see Figure 16). As the liquid flow was increased to the certain point, σ_R started to increase gradually, and small dispersed bubbles of gas could be seen flowing down through the liquid phase. This point could be designated as the onset of trickle-to-bubble flow transition. At higher liquid flow rates, size of the bubbles grew smaller as bigger bubbles broke into smaller dispersed bubbles, and more turbulence could be observed. At the point, σ_R reached a value of 1 or higher.

There was no sudden rise in the pressure drop observed at the transition. It was also seen that at such low gas flow, the onset of bubble flow is practically independent of the gas flow rate, an observation made by Honda et al [40] as well. As can be seen, the trickle to bubble flow transition appears to be taking place in the range $v_L = 15 - 18$ mm/s (L = 20 – 25 gpm).
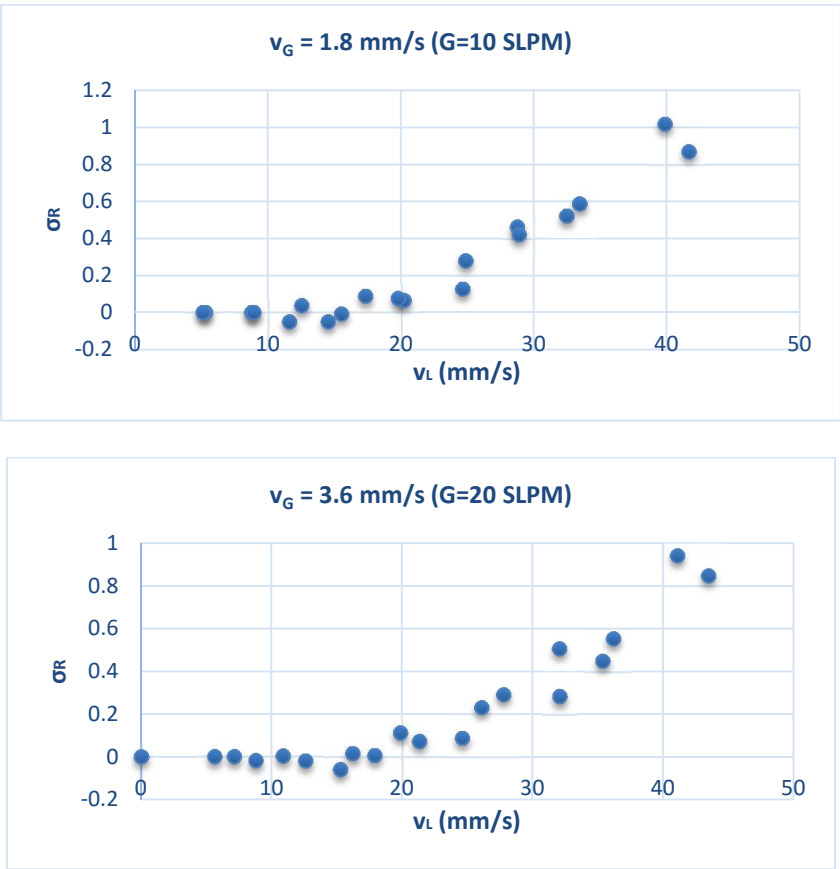

Figure 16. Variation of σ_R with v_L, for v_G =1.8 mm/s (G = 10 SLPM) and v_G = 3.6 mm/s (G=20 SLPM)

Intermediate gas flow rates: 40<G<300 SLPM (7 < vG < 54 mm/s)

At intermediate gas flow rates (see Figure 17), the trend was similar, but the value of σ_R was lesser as compared to that at lower flow rates. This can be attributed to the fact that at higher gas flow rates, gas phase is less likely to be broken down into very small dispersed bubbles. At higher gas flow rates in this range (200 SLPM – 300 SLPM), σ_R did start to regain higher values. However, visual observation did not show a bubbling behavior, but instead small local pulses near the column bottom. Therefore, this intermediate region of operation can be assumed to be where a direct transition from trickle to bubble flow regime disappears and an intermediate region exists where trickle flow, bubble flow and pulsing low regions meet (see Figure 5 for more details). This region is characterized by a turbulent rippling flow through the column at high liquid flow rates.
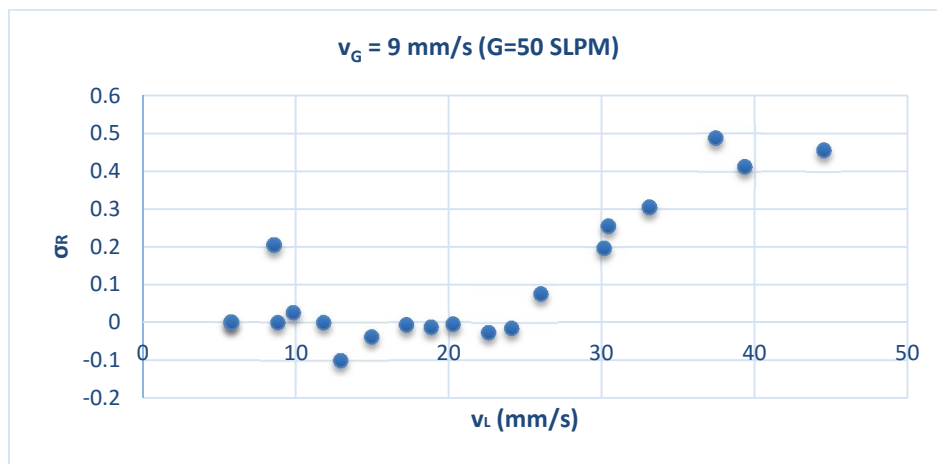

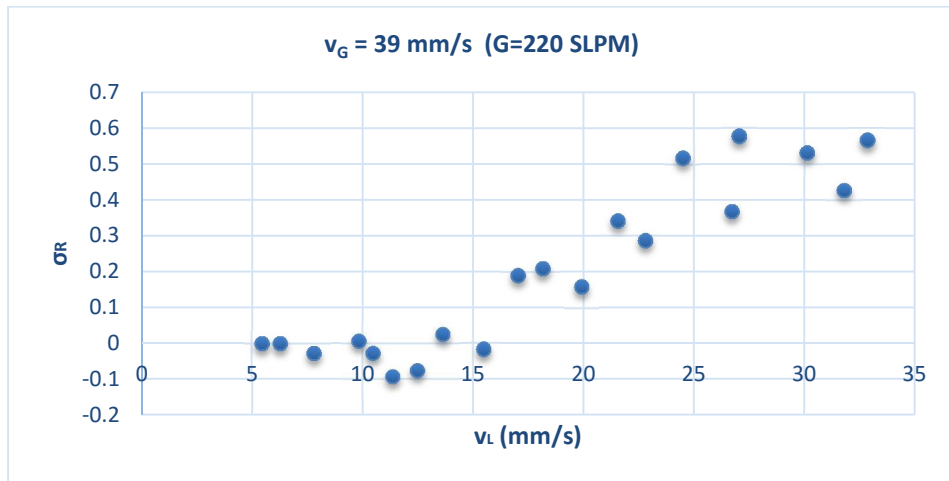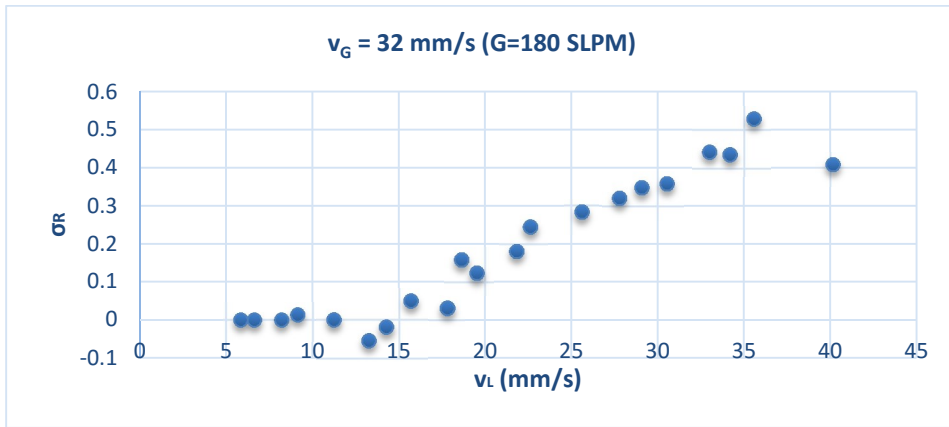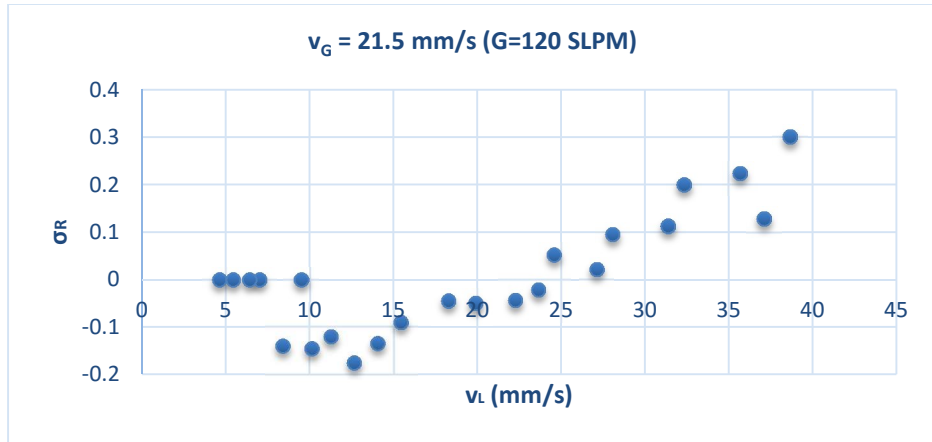**Figure 17.** Results for σ_R for the range $7 < v_G < 54$ mm/s (G = 40 – 300 SLPM)

Figure 17 Continued.

iii.   *Higher Gas Flow Rates: G > 300 SLPM (54 mm/s < v_G)*

At comparatively higher gas flow rates in the operational range studied, some level of transition from trickle flow regime to pulsing regime can be observed. At lower liquid flow rates, trickle flow prevails. At slightly higher liquid flow rates, the flow appears to be turbulent, with many small ripples through the packing, and this can be described as a 'transition' or 'rippling flow region' [56]. As liquid flow rate is increased, disturbances can be seen in the column in the form of local pulses, which can be described as small slugs of liquid flowing down arbitrarily at various locations of the column. Local pulsing has previously been reported by some researchers [55, 57, 58]. The initial pulses did not span the entire cross section of the column due to the large diameter of the column. At even higher diameters (as is the case in the industry), and at practical flow rates, it is possible that the entire pulsing flow regime may be confined to just local pulsing.

In addition, the onset of pulses was observed near the column bottom, and this incipient point of disturbance moves to the top as liquid flow is increased. This was also reported by other investigators [25, 34, 38, 59]. This is because of an increase in gas velocity due to a pressure drop through the packing. This was quantitatively supported by the standard deviation values of the pressure transducers, wherein the fluctuation values are largest for the lowermost transducer and decrease as we move up the column to other transducers.

At even higher liquid flows, the behavior differed slightly for 300 SLPM and 400 SLPM gas flow rates. Figure 18 shows the relative standard deviation trend for the

63

lowermost pressure transducer readings. For 300 SLPM, the rise is gradual, which indicates that while the operation has left the trickle flow regime, it never achieves a sharp transition to the pulsing flow regime. Rather, it enters a dispersed bubble regime at sufficiently high liquid flow rates.

For a gas flow rate of 400 SLPM (v_G = 72 mm/s), the rise in relative standard deviation is steeper and much more pronounced, which was supported by the observation of more uniform pulses across the bottom half of the packing. In addition, the height of fluctuations was higher as compared to 300 SLPM gas flow, which verifies the existing knowledge that the point of onset of pulsations moves up with an increase in liquid or gas flow rates. Also, the thickness of the pulse increased with increasing liquid flow, as reported by Christensen et al [57]. It was also observed that the pulses soon retreated to the bottom on further increasing the liquid flow, and subsequently disappeared. This verified the applicability of flow map regions which show pulsing flow regime at intermediate liquid flow rates at a fixed gas flow, and bubble flow regime at higher liquid flow rates, as the gas phase breaks into dispersed bubbles with liquid as the continuous phase [25, 34, 59].

Figure 19 shows the region on the flow map where these flow rates lie. The region just below the trickle-to-pulse flow transition line and above 300 SLPM, represents the 'transition' or 'rippling flow' region [56]. In this region, turbulent ripples can be seen in the column that cannot be clearly categorized into any particular regime. As a gas flow rate of 400 SLPM is approached, trickle-to-pulse flow transition can be observed clearly. If we define the point of trickle-to-pulse transition as the liquid flow

where σ_R becomes more than 1, then the transition for 400 SLPM gas flow occurred at

around $v_L = 17$ mm/s, or L = 23 gpm (see Figure 18(b)). This corresponds to 60,000

kg/m^2/h of liquid mass flux, which is where the transition can be seen in the flow map

(Figure 19).
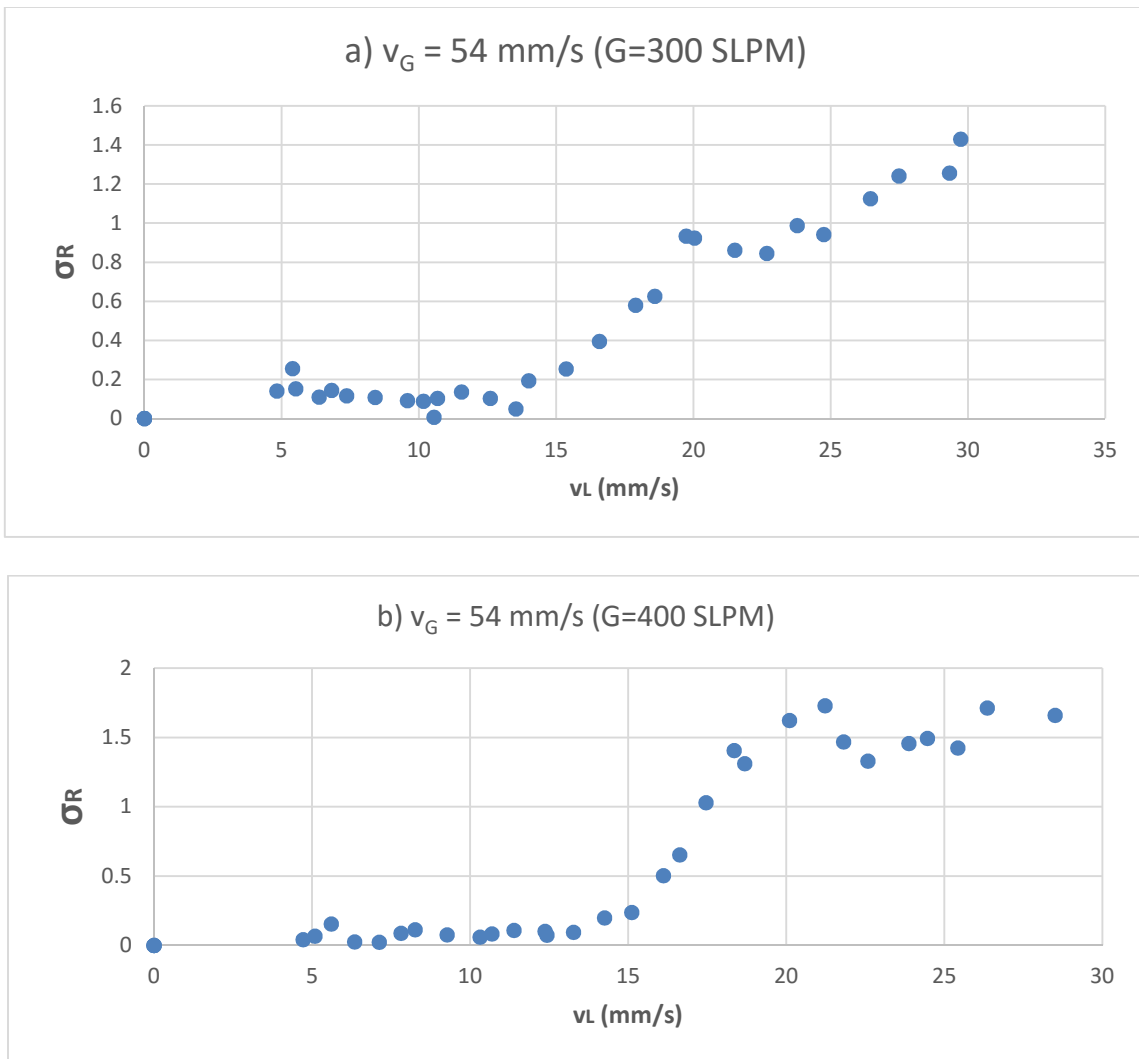
Figure 18. Variation of σ_R with liquid flow rate for (a) $v_G = 54$ mm/s (G = 300 SLPM) and (b) $v_G = 72$ mm/s (G = 400 SLPM)
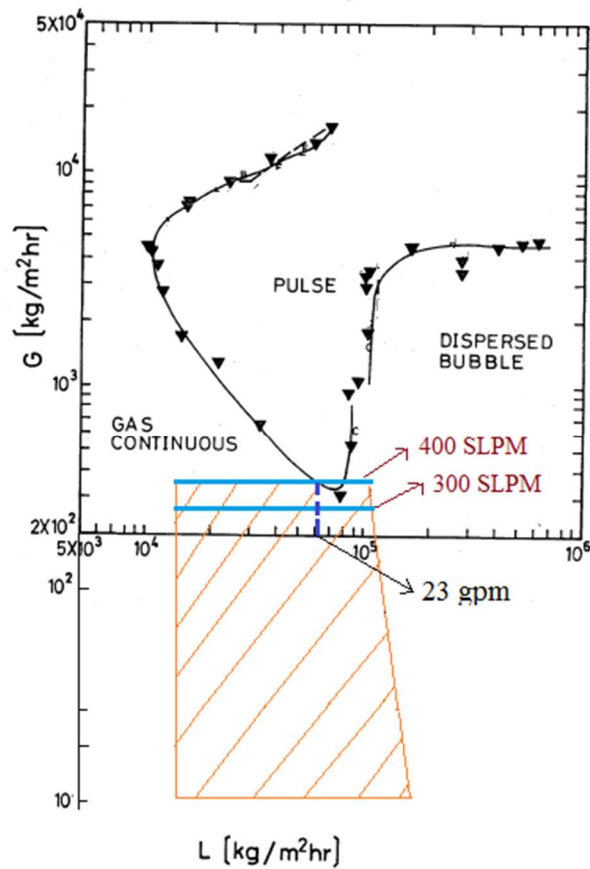
Figure 19. Location of gas flow rates 300 SLPM and 400 SLPM on the flow map by Sato et al [25]

At the low gas flow range pertinent to this study, the column did not see uniform pulses spanning the entire column, and the onset of the pulses could only reach up to the middle of the packing. It is expected that higher gas flows will yield a sharper transition to pulsing flow, with uniform alternating pulsations from top to bottom of the packing. The relative standard deviation values are also expected to be higher, as demonstrated by Honda et al, 2015 [40].

In summary, this chapter described the experimental methodology followed to collect the hydrodynamic data from the setup described in Chapter II, detailed the results obtained from the experiments, and presented a comparison of data obtained with the existing correlations covered in Chapter I. With the use of a large column with high D_C/D_P ratio (~150), cylindrical extrudate packing of high aspect ratio (~6.3), and operation at low gas superficial velocity range, the results are expected to provide a better understanding of hydrodynamics of commercial reactors at low gas flow rate operation. The last chapter summarizes the findings of this research, and suggests recommendations for future work.

CHAPTER IV

CONCLUSIONS

In this study, experiments were carried out on a large trickle bed column, to collect hydrodynamic data that can closely represent industrial scale reactor hydrodynamics. The system was set-up as described in Chapter II, with the auxiliary equipment, layers of protection, and the required instrumentation for data acquisition and control. Pressure drop, liquid holdup and flow regime transition were observed at low gas superficial velocities, and the results were compared to existing correlations in literature. The conclusions drawn from the results are summarized below:

i.   The correlations in literature disagree significantly from each other. This can be attributed to the fact that most correlations are empirical in nature, and their applicability may be confined to the range of operating conditions, packing shapes and sizes, column diameter, and fluid properties specific to the studies.

ii.   The pressure drop trend is not correctly predicted by many existing correlations. From comparison, it is clear that while it may be useful to segregate low interaction and high interaction regimes to formulate different correlations, it does not give an accurate prediction for all operating conditions.

iii. Pressure drop at low gas superficial velocities is characterized by a region of gravity drainage, wherein the liquid flow is assisted more by gravity than by the drag forces of concurrently flowing gas phase. This trend is not captured in the correlations that were analyzed in this study.

iv. Liquid Saturation increases drastically at low liquid flow rates, and reaches a saturation value at high flow rates, beyond which there is a negligible increase. A few of the correlations in literature give a fair prediction of the data, but overestimate the liquid saturation at higher liquid flow rates. A possible explanation to this phenomenon could be that most of these correlations are based on studies performed on small columns with $D_c/D_P < 10$, where substantial liquid-wall interaction can result in significant capillary forces, leading to a continuously increasing liquid holdup. For larger columns, lower liquid-wall interaction may lead to saturation of liquid holdup values at higher liquid flow rates.

v. Flow regime transition can be observed from trickle flow to dispersed bubble flow and pulsing flow, and predicted with reasonable accuracy by the existing flow maps for this operating region studied in this research. It can be inferred that flow regime transition may well be independent of column to particle diameter ratio beyond a certain value of D_c/D_P [60]. Applicability of flow maps at higher gas flow rates still needs to be verified.

vi. Trickle-to-bubble flow transition is gradual, and is clearly observed for very low gas velocities ($v_G < 7$ mm/s), where the transition is independent of the gas flow. At slightly higher gas velocities (up to $v_G \sim 50$ mm/s), the transition to bubble flow regime appears to be affected by local pulsing in the column, due to the operating conditions being in the vicinity of pulsing flow.

69

vii.   At higher gas flow rates (around $v_G \sim 70$ mm/s) in the operating range studied, transition from trickling to pulsing flow can be observed for intermediate liquid flow rates, while transition from pulse-to bubble flow regime can be visually observed for higher liquid flow rates. Trickle-to-pulse flow transition is steeper as compared to trickle-to-bubble flow.

viii.   While this study does publish novel data with respect to large column to particle diameter ratio and use of unconventional packing, applicability to commercial reactors still needs to be verified owing to different loading methodologies, fluid properties, and packing characteristics.

The experimental setup used for this study can be further employed to investigate hydrodynamics of trickle bed reactors to emulate commercial operation. Some recommendations for future work that can be as follows:

i.   Existing correlations that predict the data closely may be modified to give a better fit. Alternatively, new correlations may be developed that can closely estimate the hydrodynamic data collected from larger columns.

ii.   Data can be collected at higher gas flows, venturing into full-fledged pulsing flow regime.

iii.   Proper distribution of fluids in the bed is important for better reactor performance and heat transfer efficiency [3]. More advanced studies can be done to investigate porosity and gas-liquid distribution inside the packed bed,

using advanced experimental tools such as Capacitance/Resistance Tomography and Magnetic Resonance Imaging.

iv.   Existing theoretical models from literature may be verified by comparing with the data obtained from the setup.

REFERENCES

1.   Shah, Y.T., *Gas-liquid-solid reactor design*. Vol. 60. 1979: McGraw-Hill New York.

2.   Ramachandran, P., M. Duduković, and P. Mills, *Recent advances in the analysis and design of trickle-bed reactors.* Sadhana, 1987. 10(1-2): p. 269.

3.   Ranade, V.V., R. Chaudhari, and P.R. Gunjal, *Trickle bed reactors: Reactor engineering and applications*. 2011: Elsevier.

4.   Huang, T.C. and B.C. Kang, *Kinetic-study of naphthalene hydrogenation over Pt/Al2O3 catalyst.* Industrial & Engineering Chemistry Research, 1995. 34(4): p. 1140-1148.

5.   Hanika, J., B.N. Lukjanov, and V.A. Kirillov, *Hydrogenation of 1, 5-cyclooctadiene in a trickle bed reactor accompanied by phase transition.* Chemical Engineering Communications, 1986. 40(1-6): p. 183-194.

6.   Fishwick, R.P., R. Natividad, R. Kulkarni, P.A. McGuire, J. Wood, et al., *Selective hydrogenation reactions: A comparative study of monolith CDC, stirred tank and trickle bed reactors.* Catalysis Today, 2007. 128(1): p. 108-114.

7.   Herskowitz, M. and S. Mosseri, *Global rates of reaction in trickle-bed reactors: effects of gas and liquid flow rates.* Industrial & Engineering Chemistry Fundamentals, 1983. 22(1): p. 4-6.

8.   Wilhite, B.A., R. Wu, X. Huang, M.J. McCready, and A. Varma, *Enhancing performance of three‐phase catalytic packed‐bed reactors.* AIChE Journal, 2001. 47(11): p. 2548-2556.

9.   Meyers, R.A., *Handbook of petroleum refining processes*. 2004: McGraw-Hill.

10.   Lee, S., N. Zaborenko, and A. Varma, *Acetophenone hydrogenation on Rh/Al 2 O 3 catalyst: Flow regime effect and trickle bed reactor modeling.* Chemical Engineering Journal, 2017. 317: p. 42-50.

11.   Baldi, G., A. Gianetto, S. Sicardi, V. Specchia, and I. Mazzarino, *Oxidation of ethyl alcohol in trickle bed reactors: Analysis of the conversion rate.* The Canadian Journal of Chemical Engineering, 1985. 63(1): p. 62-66.

12. Berruti, F., R.R. Hudgins, E. Rhodes, and S. Sicardi, *Oxidation of sulfur dioxide in a trickle-bed reactor: A study of reactor modelling.* The Canadian Journal of Chemical Engineering, 1984. 62(5): p. 644-650.

13. Chuang, K.T., S. Cheng, and T. Shimin, *Removal and destruction of benzene, toluene, and xylene from wastewater by air stripping and catalytic oxidation.* Industrial & Engineering Chemistry Research, 1992. 31(11): p. 2466-2472.

14. Levec, J. and J. Smith, *Oxidation of acetic acid solutions in a trickle-bed reactor.* AIChE Journal, 1976. 22(1): p. 159-168.

15. Goto, S. and J. Smith, *Trickle-bed reactor performance. Part II. Reaction studies.* AIChE Journal, 1975. 21(4): p. 714-720.

16. Goto, S., T. Chatan, and M. Matouq, *Hydration of 2-methyl-2-butene in gas-liquid cocurrent upflow and downflow reactors.* The Canadian Journal of Chemical Engineering, 1993. 71(5): p. 821-823.

17. Leung, P., F. Recasens, and J. Smith, *Hydration of isobutene in a trickle-bed reactor: Wetting efficiency and mass transfer.* AIChE journal, 1987. 33(6): p. 996-1007.

18. Satterfield, C.N. and P.F. Way, *The role of the liquid phase in the performance of a trickle bed reactor.* AIChE Journal, 1972. 18(2): p. 305-311.

19. Kan, K.-M. and P.F. Greenfield, *Pressure drop and holdup in two-phase cocurrent trickle flows through beds of small packings.* Industrial & Engineering Chemistry Process Design and Development, 1979. 18(4): p. 740-745.

20. Dudukovic, M.P. and P. Mills, *Contacting and hydrodynamics in trickle-bed reactors.* Encyclopedia of Fluid Mechanics, 1986. 3: p. 969.

21. Colombo, A., G. Baldi, and S. Sicardi, *Solid-liquid contacting effectiveness in trickle bed reactors.* Chemical Engineering Science, 1976. 31(12): p. 1101-1108.

22. Larkins, R.P., R. White, and D. Jeffrey, *Two-phase concurrent flow in packed beds.* AIChE Journal, 1961. 7(2): p. 231-239.

23. Turpin, J.L. and R. Huntington, *Prediction of pressure drop for two-phase, two-component concurrent flow in packed beds.* AIChE Journal, 1967. 13(6): p. 1196-1202.

24.   Sato, Y., T. Hirose, F. Takahashi, and M. Toda, *Pressure loss and liquid holdup in packed bed reactor with cocurrent gas-liquid down flow.* Journal of Chemical Engineering of Japan, 1973. 6(2): p. 147-152.

25.   Sato, Y., T. Hirose, F. Takahashi, M. Toda, and Y. Hashiguchi, *Flow pattern and pulsation properties of cocurrent gas-liquid downflow in packed beds.* Journal of Chemical Engineering of Japan, 1973. 6(4): p. 315-319.

26.   Charpentier, J.C. and M. Favier, *Some liquid holdup experimental data in trickle-bed reactors for foaming and nonfoaming hydrocarbons.* AIChE Journal, 1975. 21(6): p. 1213-1218.

27.   Midoux, N., M. Favier, and J.C. Charpentier, *Flow pattern, pressure loss and liquid holdup data in gas-liquid downflow packed beds with foaming and nonfoaming hydrocarbons.* Journal of Chemical Engineering of Japan, 1976. 9(5): p. 350-356.

28.   Specchia, V. and G. Baldi, *Pressure drop and liquid holdup for two phase concurrent flow in packed beds.* Chemical Engineering Science, 1977. 32(5): p. 515-523.

29.   Chou, T., F. Worley, and D. Luss, *Transition to pulsed flow in mixed-phase cocurrent downflow through a fixed bed.* Industrial & Engineering Chemistry Process Design and Development, 1977. 16(3): p. 424-427.

30.   Fukushima, S. and K. Kusaka, *Interfacial area and boundary of hydrodynamic flow region in packed column with cocurrent downward flow.* Journal of Chemical Engineering of Japan, 1977. 10(6): p. 461-467.

31.   Clements, L. and P. Schmidt, *Two-phase pressure drop in cocurrent downflow in packed beds: Air-silicone oil systems.* AIChE Journal, 1980. 26(2): p. 314-317.

32.   Clements, L. and P. Schmidt, *Dynamic liquid holdup in two-phase downflow in packed beds: Air-silicone oil system.* AIChE Journal, 1980. 26(2): p. 317-319.

33.   Mills, P. and M. Dudukovic, *Evaluation of liquid-solid contacting in trickle-bed reactors by tracer methods.* AIChE Journal, 1981. 27(6): p. 893-904.

34.   Blok, J., J. Varkevisser, and A. Drinkenburg, *Transition to pulsing flow, holdup and pressure drop in packed columns with cocurrent gas-liquid downflow.* Chemical Engineering Science, 1983. 38(5): p. 687-699.

35.   Levec, J., A.E. Saez, and R. Carbonell, *The hydrodynamics of trickling flow in packed beds. Part II: Experimental observations.* AIChE Journal, 1986. 32(3): p. 369-380.

36.   Ellman, M.J., N. Midoux, A. Laurent, and J.C. Charpentier, *A new, improved pressure drop correlation for trickle-bed reactors.* Chemical Engineering Science, 1988. 43(8): p. 2201-2206.

37.   Wammes, W., S. Mechielsen, and K. Westerterp, *The influence of pressure on the liquid hold-up in a cocurrent gas-liquid trickle-bed reactor operating at low gas velocities.* Chemical Engineering Science, 1991. 46(2): p. 409-417.

38.   Wammes, W., S. Mechielsen, and K. Westerterp, *The transition between trickle flow and pulse flow in a cocurrent gas—liquid trickle-bed reactor at elevated pressures.* Chemical Engineering Science, 1990. 45(10): p. 3149-3158.

39.   Wang, R., Z. Mao, and J. Chen, *A study of trickling-to-pulsing flow transition in trickle-bed reactors (TBR).* Chemical Engineering Communications, 1994. 127(1): p. 109-123.

40.   Honda, G.S., E. Lehmann, D.A. Hickman, and A. Varma, *Effects of Prewetting on Bubbly-and Pulsing-Flow Regime Transitions in Trickle-Bed Reactors.* Industrial & Engineering Chemistry Research, 2015. 54(42): p. 10253-10259.

41.   Sodhi, V. and A. Bansal, *Analysis of Foaming Flow Instabilities for Dynamic Liquid Saturation in Trickle Bed Reactor.* Analysis, 2011. 356: p. 2736.

42.   Sicardi, S., H. Gerhard, and H. Hoffmann, *Flow regime transition in trickle-bed reactors.* The Chemical Engineering Journal, 1979. 18(3): p. 173-182.

43.   Larachi, F., I. Iliuta, M. Chen, and B.P.A Grandjean, *Onset of pulsing in trickle beds: evaluation of current tools and state-of-the-art correlation.* The Canadian Journal of Chemical Engineering, 1999. 77(4): p. 751-758.

44.   Reinecke, N. and D. Mewes, *Investigation of the two-phase flow in trickle-bed reactors using capacitance tomography.* Chemical Engineering Science, 1997. 52(13): p. 2111-2127.

45.   Gianetto, A. and V. Specchia, *Absorption in packed towers with concurrent downward high-velocity flows: I-interfacial areas.* Quaderni Dell'ingegnere Chimico Italiano, 1970. 6: p. 125-133.

46.   Ergun, S. and A.A. Orning, *Fluid flow through randomly packed columns and fluidized beds.* Industrial & Engineering Chemistry, 1949. 41(6): p. 1179-1184.

47.   Lockhart, R. and R. Martinelli, *Proposed correlation of data for isothermal two-phase, two-component flow in pipes.* Chem. Eng. Prog, 1949. 45(1): p. 39-48.

48.   Tallmadge, J., *Packed bed pressure drop—an extension to higher Reynolds numbers.* AIChE Journal, 1970. 16(6): p. 1092-1093.

49.   Charpentier, J., C. Prost, W. Van Swaaij, and P. Le Goff, *Étude de la rétention de liquide dans une colonne à garnissage arrosé à co-courant et à contre-courant de gaz–liquide.* Chimie & Industrie–Génie Chimique, 1968. 99: p. 803-811.

50.   Gianetto, A., G. Baldi, V. Specchia, and S. Sicardi, *Hydrodynamics and solid-liquid contacting effectiveness in trickle-bed reactors.* AIChE Journal, 1978. 24(6): p. 1087-1104.

51.   Otake, T. and K. Okada, *Liquid hold-up in packed towers—operating hold-up without gas flow.* Kagaku Kogaku, 1953. 17: p. 176.

52.   Goto, S. and J. Smith, *Trickle-bed reactor performance. Part I. Holdup and mass transfer effects.* AIChE Journal, 1975. 21(4): p. 706-713.

53.   Van Swaaij, W., J. Charpentier, and J. Villermaux, *Residence time distribution in the liquid phase of trickle flow in packed columns.* Chemical Engineering Science, 1969. 24(7): p. 1083-1095.

54.   Ramachandran, P. and R. Chaudhari, *Three-phase catalytic reactors.* Vol. 2. 1983: Gordon & Breach Science Pub.

55.   Anadon, L.D., A.J. Sederman, and L.F. Gladden, *Rationalising MRI, conductance and pressure drop measurements of the trickle-to-pulse transition in trickle beds.* Chemical Engineering Science, 2008. 63(19): p. 4640-4648.

56.   Weekman, V.W. and J.E. Myers, *Fluid-flow characteristics of concurrent gas-liquid flow in packed beds.* AIChE Journal, 1964. 10(6): p. 951-957.

57.   Christensen, G., S. McGovern, and S. Sundaresan, *Cocurrent downflow of air and water in a two-dimensional packed column.* AIChE Journal, 1986. 32(10): p. 1677-1689.

58.   Sederman, A. and L. Gladden, *Transition to pulsing flow in trickle-bed reactors studied using MRI.* AIChE Journal, 2005. 51(2): p. 615-621.

59.   Wilhite, B., B. Blackwell, J. Kacmar, A. Varma, and M.J. McCready, *Origins of pulsing regime in cocurrent packed-bed flows.* Industrial & Engineering Chemistry Research, 2005. 44(16): p. 6056-6066.

60.   Herskowitz, M. and J. Smith, *Trickle-bed reactors: A review.* AIChE Journal, 1983. 29(1): p. 1-18.